CHALMERS
UNIVERSITY OF TECHNOLOGY

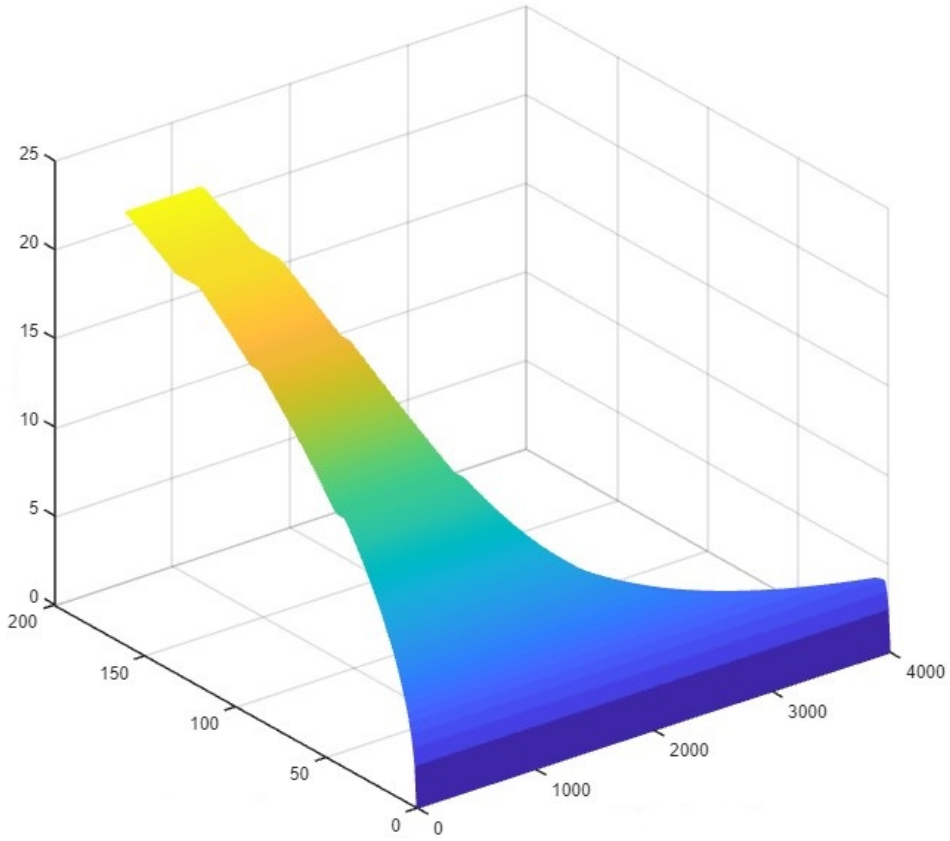

Induction Machine Flux Control during Transient Operation

MAYUR SHARMA
SUCHET SUBBA RAO KULKARNI

DEPARTMENT OF ELECTRICAL ENGINEERING

CHALMERS UNIVERSITY OF TECHNOLOGY
Gothenburg, Sweden 2024
www.chalmers.se

Master's thesis 2024

Induction Machine Flux Control during Transient Operation

MAYUR SHARMA
SUCHET SUBBA RAO KULKARNI

CHALMERS
UNIVERSITY OF TECHNOLOGY

Department of Electrical Engineering
Division of Electric Power Engineering
Chalmers University of Technology
Gothenburg, Sweden 2024

Induction Machine Flux Control during Transient Operation
MAYUR SHARMA
SUCHET SUBBA RAO KULKARNI

Supervisor: Joachim Härsjö, Volvo Car Corporation
Examiner: Stefan Lundberg, Electric Power Engineering

Master's Thesis 2024
Department of Electrical Engineering
Division of Electric Power Engineering
Chalmers University of Technology
SE-412 96 Gothenburg
Telephone +46 31 772 1000

Cover: 3D plot showing how the MTPA points of i_{sd} change with respect to the speed and torque of an induction machine

Typeset in LaTeX
Printed by Chalmers Reproservice
Gothenburg, Sweden 2024

Abstract

This thesis investigates control methodologies for induction machines during transient operations, focusing on the implementation of active flux and torque current control strategies while emphasising energy efficiency and optimal performance. It begins by identifying the steady-state operating points that minimise copper losses, known as Maximum Torque per Ampere (MTPA) points. To find these points, the goal is to maximise the machine's torque equation while considering the current and voltage equations as constraints. This is further solved as a constrained optimisation problem using MATLAB. Further, based on FOC principles the machine as well as the controller are modelled in inverse Γ-form dq reference frame using Simulink. To analyse the machine's performance between two steady-state operating points, this work extends the application of MTPA to transient scenarios where rapid flux changes are necessary for responsive torque adaptation. The work explores the usage of active flux and torque control ideas by investigating the trade-offs involved in controlling i_{sd} and/or i_{sq}.

The findings from this study are valuable in the development of control strategies for an induction machine in automotive drive systems. The study shows that using a PI-based flux controller accelerates the magnetisation and demagnetisation process. However, it is found that stable flux control is achieved in Field Weakening region when a field weakening controller is used. Furthermore, torque control mitigates the noticeable delay in torque production despite using active flux control during rapid and high torque demands. In these situations, additional compensation in i_{sq} is necessary to offset the lag. However, this comes with a trade-off: the copper losses increase due to deviations from MTPA trajectory in both i_{sd} and i_{sq}. Nevertheless, this strategy ensures an instantaneous torque response.

Thus, employing a control strategy depends on multiple factors such as prioritising energy efficiency or performance, considering the machine's operating state, and accounting for the resulting voltage and current constraints. Since no single strategy satisfies all requirements equally, the appropriate strategy should be chosen based on the preferred trade-off between energy efficiency and performance while also considering the machine's operating conditions.

Keywords: Induction Machine, MTPA, Transient control, Flux control, Torque control, Energy efficiency, trade-off analysis

Acknowledgements

This research work was carried out at Volvo Car Corporation in collaboration with Chalmers University of Technology's Electric Power Engineering department. We want to thank our supervisor and examiner Stefan Lundberg, for his valuable guidance throughout the thesis. We really appreciate his support. We also thank Joachim Härsjö from Volvo Cars for his mentorship and valuable insights. We also thank Shayan Halder for his critical inputs. Lastly, we are very grateful to our parents for their support throughout this project.

Mayur Sharma, Suchet Subba Rao Kulkarni, Gothenburg, October 2024

Contents

1
Introduction

1.1 Background

The operation of electric machines can be classified into two primary modes: steady-state and transient. Steady-state operation refers to conditions where the machine operates at a constant speed and under a consistent load. Conversely, transient operations are scenarios characterised by sudden changes in speed, torque or load, challenging the machine's ability to adapt its performance. This is common in automotive applications, where the drive system leaves its previous stable operating condition to settle in a new steady state due to variations in torque within a short time interval [1]. Thus, controlling induction machines (IM) efficiently requires sophisticated control strategies. Among the prevalent methods, scalar control is a straightforward approach which regulates the amplitude of voltage and frequency supplied to the machine. While suitable for basic applications, it lacks the precision demanded by more advanced systems such as drive systems for EV's. In contrast, vector control allows precise manipulation of torque and flux. One such method is field-oriented control (FOC) which independently controls the magnetizing and torque producing components of the stator current [2].

Maximum Torque per Ampere (MTPA) are steady-state points which maximise torque production relative to stator current magnitude, thus ensuring lower energy losses at these points. Unlike a Permanent Magnet Synchronous Machine (PMSM) which has a constant magnetic flux due to the permanent magnets, the magnetic flux in an IM has to be induced in the rotor, making the flux controllable indirectly through stator current control. Hence it is a complex relationship between the components of stator current (i_{sd} and i_{sq}), rotor flux, and torque production [3]. Controlling IM's on MTPA points only ensure low energy losses at steady-state operation. During transient periods, to maintain instantaneous response from the machine, the flux producing (i_{sd}) and torque producing (i_{sq}) currents need to be precisely controlled [4]. A strategy to cover this transient operation is investigated in this work.

1.2 Aim

The main focus of this thesis is to design and evaluate control methods for transitions in an induction machine drivetrain between different steady-state MTPA operating points, while keeping the energy consumption low and maintaining a good dynamic performance. The trade-offs as, the transient current consumption and the resulting copper and iron losses due to stator current magnitude and changes in flux respectively, are considered for the various strategies.

1.3 Limitations

Given the aim and background of this thesis, this section outlines the areas not covered under the scope

i. **Investigation into alternate control techniques:** This study focuses on extending the MTPA based FOC method to transient conditions. However, it does not include a comparative analysis with other vector control methods such as Direct Torque Control (DTC) or Model Predictive Control (MPC), which might offer alternative solutions.

ii. **Limited consideration on inverter operation:** The interaction of proposed control strategy with inverter operation such as, high frequency switching and related modulation effects among others are not studied.

iii. **Practical implementation aspects:** The study acknowledges the importance of implementing the proposed control strategy but does not account for the challenges associated with real world deployment - hardware platforms and Digital Signal Processors (DSP) which are commonly used in a drivetrain.

iv. **Battery dynamics:** While the design of the control strategy takes into account voltage and current limits, it does not fully explore the non-linear behaviour of battery electrical parameters such as State of Charge (SOC) which changes with time.

v. **Thermal aspects of the machine:** The study does not focus on examining the associated thermal responses of the machine components such as winding temperatures.

2

Induction machine modeling and control

In this chapter, the approach to build a mathematical model of the IM is described first. Further, concepts related to the operation of the machine are highlighted where the theoretical background to MTPA, Field Weakening and Maximum Torque per Voltage (MTPV) are briefly explained. The work is built on these principles in the later sections while explaining the control methods employed.

2.1 Machine Modelling

The mathematical modelling of induction machines using equivalent circuit parameters simplifies the study of its control operation. Two primary modelling approaches are evaluated. Using the T model simplifies the machine to an extent, but it can be complex to work with if magnetic non-linearity is included [5]. This is because of complexity introduced to estimate the rate of change of inductance due to a varying flux. The model is also over parameterised for vector control applications, which are most commonly used in automotive drive systems [2]. On the other hand, the inverse-Γ model is a simplification of the T model without sacrificing essential information such as dynamic flux linkage and it allows for a clearer representation of the effects of control actions on the machine's behavior [5]. In this work, the inverse-Γ model is used to derive the equations for both the machine and its controllers, such as the current and speed controllers. This approach is chosen because it ensures uniformity and simplicity while also capturing the inherent physics of the machine. By modeling both the machine and controller in the dq reference frame using the inverse-Γ model, a consistent and effective representation of the system's dynamics is achieved.

The vector control methods, evaluated in Subsection 2.2, are the most widely adopted techniques for controlling AC machine drivetrains [2]. These methods require calculations of the machine parameters. AC machines, such as an IM, have sinusoidal currents and voltages that change over time, making these calculations mathematically complex. To simplify this process in the control domain, Clarke and Park transformations are used.

The Clarke transformation is a mathematical tool used to convert three-phase quantities into two-phase quantities in a stationary reference frame. In an induction

machine, the stator voltage is a complex number as indicated by the bar under $\underline{u}_s$ represented in (2.5). After applying the Clarke transformation, the stator voltage can be split into real and imaginary parts, corresponding to the α and β components [6]. This transformation reduces the complexity of three-phase systems by representing them with two orthogonal components, α and β. The visual representation of Clarke transformation is shown in Figure 2.1.

In a three-phase system, the currents I_a, I_b and I_c are typically 120° out of phase with each other. The Clarke transformation re-maps these three-phase currents onto a two-dimensional plane using the following equations:

$$I_\alpha = I_a \tag{2.1}$$

$$I_\beta = \frac{1}{\sqrt{3}} I_a + \frac{2}{\sqrt{3}} I_b \tag{2.2}$$

This specific transformation is amplitude-invariant, meaning the magnitude of the resultant two-phase system is the same as that of the original three-phase system. Choosing this transformation maintains power consistency across the model.

The Park transformation further simplifies the analysis by converting stationary two-phase α and β quantities into a rotating reference frame, represented as the dq system [7]. This transformation aligns the rotating vectors with the reference frame of the machine, facilitating easier analysis and control. Once the two-phase quantities are obtained from the Clarke transformation, the Park transformation is applied to convert them into the rotating frame using the following equations:

$$I_d = I_\alpha \cos(\theta) + I_\beta \sin(\theta) \tag{2.3}$$

$$I_q = -I_\alpha \sin(\theta) + I_\beta \cos(\theta) \tag{2.4}$$

Here, θ represents the angle of rotation, which corresponds to the rotor flux angle in an induction machine. The resulting I_d and I_q components represent the d and q axis components, respectively shown in Figure 2.1.

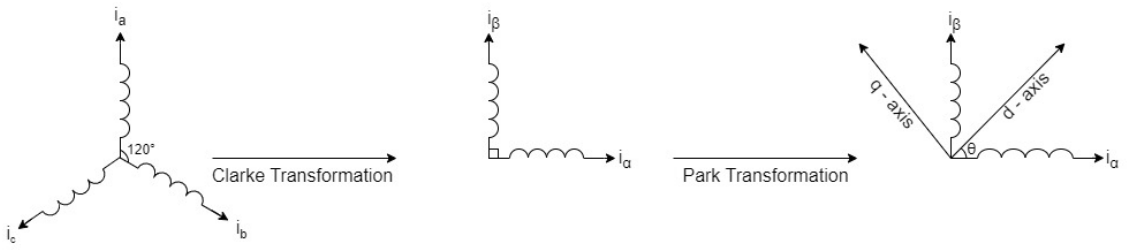

Figure 2.1: Phase Transformation principle: 3 Phase to dq

The dynamic inverse-Γ Model Equivalent Circuit of the IM in the dq reference frame is shown in Figure 2.2 [13].

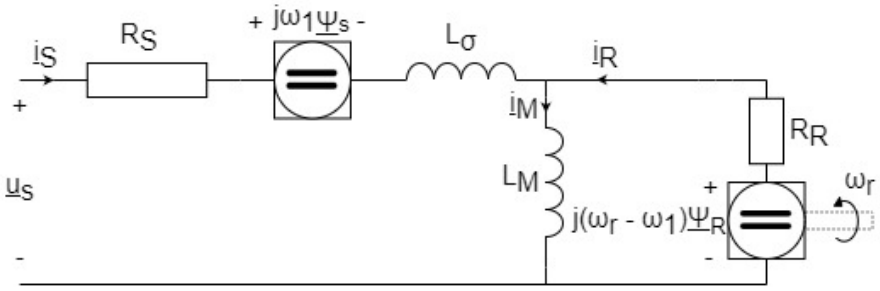

Figure 2.2: Inverse-Γ Model Equivalent Circuit of the IM

By expressing voltages, currents and flux linkages in the *dq* reference frame, i.e. as complex vectors, the inverse-Γ Model of the IM can be written as [13]:

$$\underline{u}_s = (R_s + R_R + j\omega_1 L_\sigma)\,\underline{i}_s + L_\sigma \frac{d\underline{i}_s}{dt} + \left(j\omega_r - \frac{R_R}{L_M}\right)\underline{\psi}_R \tag{2.5}$$

$$\frac{d\underline{\psi}_R}{dt} = R_R \underline{i}_s - (\frac{R_R}{L_M} + j(\omega_1 - \omega_r))\underline{\psi}_R \tag{2.6}$$

$$T_e = \frac{3}{2} n_p (\psi_{Rd} i_{sq} - \psi_{Rq} i_{sd}) \tag{2.7}$$

$$\omega_r = \Omega_r n_p \tag{2.8}$$

Where,

$\underline{u}_s$: Stator voltage (V)
R_s : Stator winding resistance (Ω)
R_R : Rotor winding resistance (Ω)
ω_1 : Slip speed (rpm)
L_σ : Stator leakage inductance (H)
$\underline{i}_s$: Stator current (A)
ω_r : Electrical speed of rotor (rad/s)
L_M : Mutual inductance (H)
$\underline{\psi}_R$: Rotor flux linkage (Wb)
$\frac{d\underline{\psi}_R}{dt}$: Rate of change of Flux linkage (Wb/s)
T_e : Electrodynamical torque output (Nm)
n_p : Number of pole pairs
ψ_{R_d} : d-axis rotor flux linkage component (Wb)
ψ_{R_q} : q-axis rotor flux linkage component (Wb)
i_{sd} : d-axis stator current component (A)
i_{sq} : q-axis stator current component (A)
Ω_r : Mechanical speed of rotor (rad/s)

If the d-axis is aligned with the rotor flux linkage ($\psi_{R_q} = 0$), these equations can be simplified to,

$$v_{sd} = (R_s + R_R)i_{sd} + L_\sigma \frac{di_{sd}}{dt} - \omega_1 L_\sigma i_{sq} - \frac{R_R}{L_M}\psi_{Rd} \tag{2.9}$$

$$v_{sq} = (R_s + R_R)i_{sq} + L_\sigma \frac{di_{sq}}{dt} + \omega_1 L_\sigma i_{sd} + \omega_r \psi_{Rq} \tag{2.10}$$

$$\frac{d\psi_{Rd}}{dt} = R_R i_{sd} - \frac{R_R}{L_M}\psi_{Rd} \tag{2.11}$$

$$T_e = \frac{3}{2} n_p \psi_{Rd} i_{sq} \tag{2.12}$$

Equations (2.9) and (2.10) have been derived by splitting (2.5) into its real and imaginary part using the relations $\underline{u}_s = u_{s_d} + j u_{s_q}$, $\underline{i}_s = i_{s_d} + j i_{s_q}$ and $\underline{\psi}_R = \psi_{R_d}$. In steady state (2.11) is equal to,

$$\psi_{Rd} = L_M i_{sd} \tag{2.13}$$

From this it can be noticed that the d-component of the stator current magnetizes the machine (gives the rotor flux magnitude) and from (2.12) that the q-component generates torque.

2.2 Selection of dq-currents for different operating conditions

The simplified torque equation for an IM is represented by (2.12) shows that along with the pole-pair number, both the i_{sq} and ψ_{Rd} components contribute to produce torque. This implies that various combinations of i_{sd} and i_{sq} can result in the same torque.

2.2.1 Maximum Torque Per Ampere (MTPA)

Calculating all sources of power losses can be challenging due to their complexity and the need for advanced models. However, since Joule losses (I^2R) are the most substantial [8], this study focuses on them. The MTPA concept aims to minimise the total current magnitude for a given value of torque and thereby minimizing the Joule losses. It is achieved by determining the optimal ratio of i_{sd} to i_{sq}, which ensures the required level of flux in the machine while delivering the desired torque. By doing so, the operating points along the machine's torque-speed curve are set and they represent the stable states where the machine can efficiently operate to meet various torque and speed requirements.

The MTPA trajectory can be found in steady state by using (2.12) and (2.13) along with the current constraint [9], which is the physical limit of the inverter, by expressing the dq currents in polar form as:

$$i_{sd} = I_s \cos(\beta) \tag{2.14}$$
$$i_{sq} = I_s \sin(\beta) \tag{2.15}$$

where β is the angle of the current vector and,

$$I_s = \sqrt{i_{sd}^2 + i_{sq}^2} \tag{2.16}$$

is the current magnitude. In steady state (2.13) can be substituted into (2.12),

$$T_e = 1.5 n_p L_M i_{sd} i_{sq} \tag{2.17}$$

Using (2.14), (2.15) and the trigonometric identity $\cos(\beta)\sin(\beta) = \frac{1}{2}\sin(2\beta)$, (2.17) can be rewritten as

$$T_e = 1.5 n_p L_M I_s^2 \frac{1}{2} \sin(2\beta) \tag{2.18}$$

To determine the optimal current angle β that results in maximum torque, the torque expression in (2.18) should be differentiated with respect to β,

$$\frac{dT_e}{d\beta} = 1.5 n_p L_M I_s^2 \cos(2\beta) = 0$$

When $\beta = 45°$, this is zero and the torque in (2.18) has its maximum and for this angle, it is mathematically observed that $i_{sd} = i_{sq}$. This relationship holds true for all current magnitudes up to the rated current, $I_s \leq I_{s,rated}$. However, operating the machine continuously above its rated current is not desirable because it could lead to overheating and potential damage to the machine.

Figure 2.3 depicts the MTPA region, describing the constant torque lines, pink MTPA trajectory, current limit and the voltage limit circle. These define the feasible operating region for the machine. The constant torque lines represent different levels of torque that the machine can generate, with each line indicating a specific torque level where the torque remains constant but the magnitude and angle of the current vector can change. The pink MTPA trajectory shows the optimal path for minimizing losses as it intersects the constant torque lines at points where the machine operates with minimal currents to produce the given torque. At this angle of the trajectory, the machine achieves the lowest possible losses because it minimizes the total stator current required to produce a given torque. The current limit circle is defined by the equation:

$$I_s^2 \leq i_{sd}^2 + i_{sq}^2 \tag{2.19}$$

it defines the maximum current the machine can safely draw without exceeding its rated limit. As the machine follows the MTPA trajectory toward point A, it eventually intersects the current limit circle. At point A, the machine reaches its rated torque which is the highest torque it can sustain continuously without overheating. This point is crucial because it marks the point where the machine must shift from MTPA control.

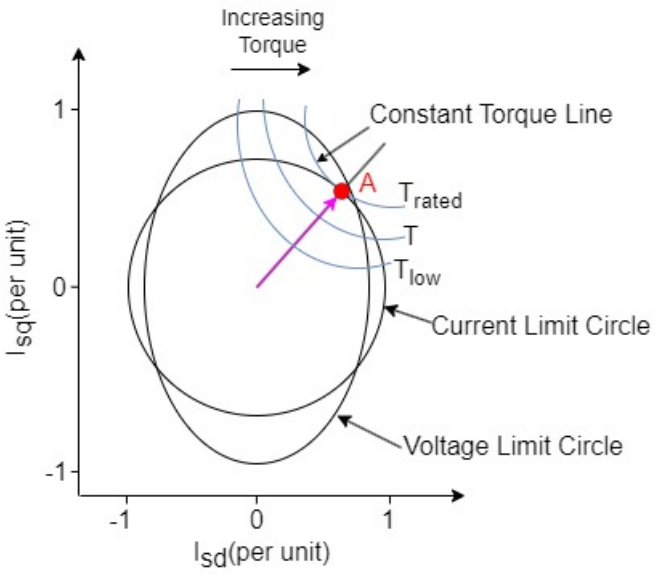

Figure 2.3: MTPA region current and voltage circles

2.2.2 Field weakening

The back-emf term $(j\omega_r - \frac{R_R}{L_M})\underline{\psi}_R$ in (2.5) is dependant on speed, meaning that as the rotor speed increases, the back-emf also increases proportionally. This causes the usable voltage to be constrained by the machine's rated voltage, as described by

$$V_{s_{\text{rated}}}^2 \leq V_{sd}^2 + V_{sq}^2 \tag{2.20}$$

To increase the machine's speed beyond the point where the voltage magnitude reaches the rated voltage, field weakening must be used. This involves reducing the rotor flux magnitude by decreasing i_{sd}. In Figure 2.3, the voltage limit circle represents combinations of d and q currents that result in the machine's rated voltage magnitude, as described by (2.20) at a specific speed. As the machine's speed increases, the radius of the voltage circle decreases, as seen in Figure 2.4, which reflects the shrinking available voltage due to the higher back-emf. This shrinking effect which defines the boundaries within which the machine can operate effectively at higher speeds.

The path from point B to point C deviates from the MTPA trajectory because the machine is now operating in the field weakening region. As the voltage limit continues to shrink, the machine can no longer follow the optimal MTPA path, which lies outside the voltage limit circle at higher speeds.

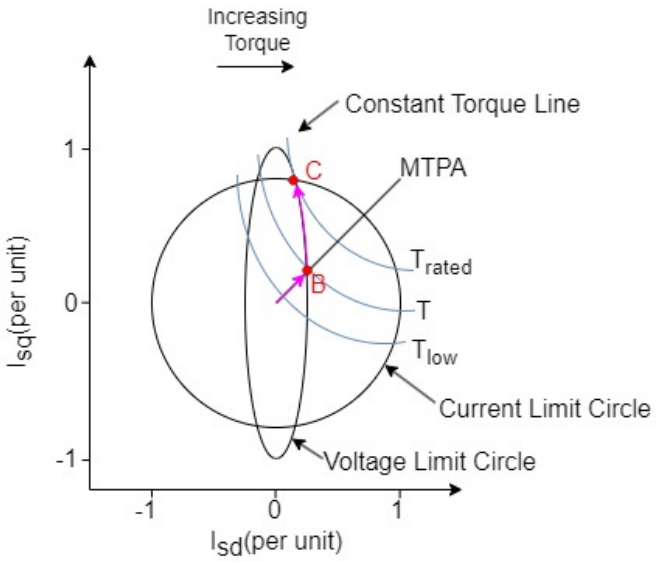

Figure 2.4: Field Weakening region current and voltage circles

Hence, between points B and C, the machine follows a smooth curve along the voltage limit circle. This curve represents a transition where i_{sd} is gradually reduced and i_{sq} is increased to maintain the highest possible torque output within the constrained voltage limits.

2.2.3 Maximum Torque Per Voltage (MTPV)

In the very high-speed region of a machine, more field weakening is required to suppress the back-emf. However, it is not efficient to go very low on flux as that will significantly limit the torque that can be produced at very high speeds.

In the Maximum Torque Per Voltage (MTPV) region, the torque generated by the machine is constrained not by the maximum usable current but by the available voltage. As shown in Figure 2.5, when the machine operates at very high speeds, the voltage limit circle shrinks within the current limit circle due to increased back-emf. This shrinking voltage circle means a smaller feasible operating region where the machine can operate effectively constrained by the available voltage. Point E in Figure 2.5 represents the maximum torque that the machine can produce within its operational limits at a given speed. Within the voltage circle, the most efficient operation is achieved when the current follows the MTPA trajectory, indicated by the pink line extending from the center of the voltage circle towards point D. The segment between points D and E lies on the boundary of the voltage circle, as described by (2.20). In the MTPV region, to produce maximum torque, the current trajectory must adhere to this boundary, described by the pink line from point D to point E.

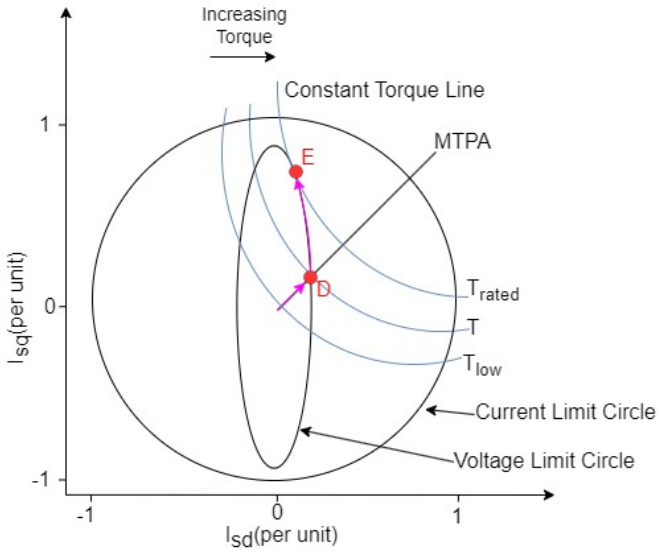

Figure 2.5: MTPV region current and voltage circles

Beyond point E, if the machine's speed increases further, the operating limit shrinks even more within the voltage circle as its radius continues to reduce. This reduction in the voltage circle's radius limits the available torque, further constraining the machine's performance at higher speeds.

3
Simulation model

This chapter begins by introducing the methodology used to determine the steady-state operating points considering MTPA. The operating points are found by formulating the machine's torque, voltage, and current equations as a constrained optimisation problem using Matlab. Additionally, the dynamic simulation model of the induction machine drive system is discussed. This model is used for testing the different methods for how to make the transition between the steady state MTPA operating points in an energy efficient way, while maintaining a good dynamic performance.

It is then observed that operating at MTPA points during transients results in a slow torque response, highlighting the importance of having a dedicated strategy which makes the machine more responsive.

3.1 MTPA scripting

In order to extract maximum efficiency from the machine, one approach can be to optimise its operational points and MTPA is a strategy that aligns with this idea which is explained in Chapter 2. The approach to finding the operating points can be summarised as follows

1. **Objective:** Maximise the torque output per unit of current by adjusting the phase angle between the stator current and the rotor magnetic field.
2. **Constraint:** Operate within defined electrical limits (voltage and current) to ensure safe and reliable performance across all operational states.

A typical strategy is to approach the torque equation as a constrained optimisation problem. The *fmincon* function in MATLAB which stands for "find minimum of constrained nonlinear multivariable function," is specifically designed for this type of problem-solving [10]. In the context of MTPA, this implies to maximise the torque equation while using the least amount of current, all within the operational constraints such as voltage and current limits.

3.1.1 Machine parameters

The induction machine studied in this thesis is a 15kW, 6-pole machine with parameters described in Table 3.1. The machine parameters are taken from the course

FEM-based design of electrical machines - EEN125 at Chalmers. The stator inductance for this machine is derived from an existing Finite Element Model generated in Ansys Maxwell. The obtained variation of stator inductance (L_s) with respect to the stator current magnitude (I_s) is illustrated in Figure 3.1.

Table 3.1: Machine Parameters

Machine Parameters (Units)	**Value**
Rotor Winding Resistance R_r (Ω)	0.190
Stator Winding Resistance R_s (Ω)	0.184
Stator Leakage Inductance $L_{s\lambda}$ (H)	2.2×10^{-3}
Rotor Leakage Inductance $L_{r\lambda}$ (H)	2.65×10^{-3}
Pole Pair Number n_p	3
Rated Phase Voltage V_{rated} (V)	250
Rated Phase Current I_s (A)	45
Max mechanical Rotor speed n_r (RPM)	4000

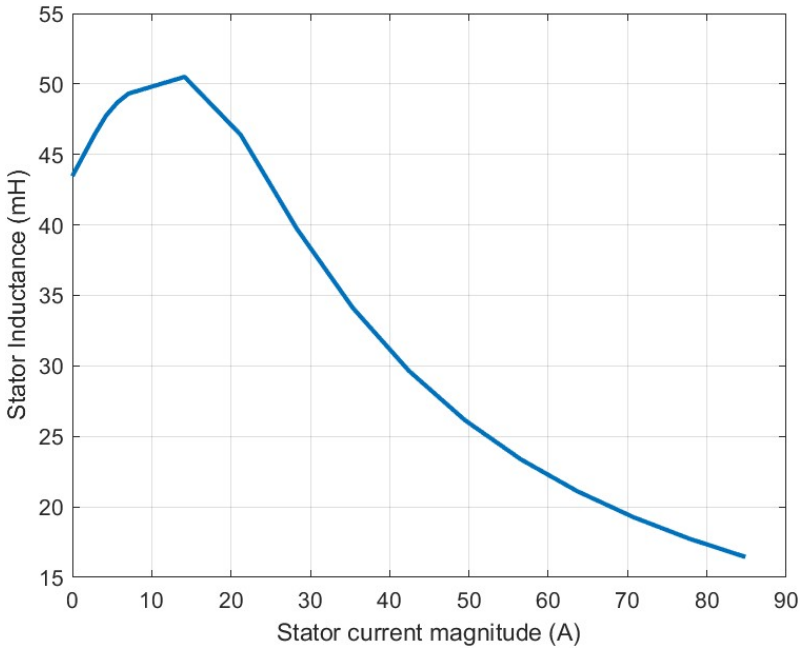

Figure 3.1: Variation of Stator Inductance with Stator current magnitude

To calculate the variation of magnetising or mutual inductance (L_m) across the entire current magnitude range, the constant values for rotor ($L_{r\lambda}$) and stator ($L_{s\lambda}$) leakage inductances from Table 3.1 are considered in

$$L_s = L_{s\lambda} + L_m \tag{3.1}$$

$$L_r = L_{r\lambda} + L_m \tag{3.2}$$

These quantities, along with the rotor resistance (R_r) from Table 3.1 are used to determine the inverse-Γ form parameters of the machine by using (3.3), (3.4), (3.5) and (3.6)

$$L_M = \frac{L_m^2}{L_r} \tag{3.3}$$

$$L_\sigma = L_s - L_M \tag{3.4}$$

$$R_R = \left(\frac{L_m}{L_r}\right)^2 R_r \tag{3.5}$$

$$\underline{\psi}_R = \frac{L_m}{L_r}\underline{\psi}_r \tag{3.6}$$

Figure 3.2 shows the variation of L_M with ψ_{Rd}. Since an inductor is a current-stiff element, the magnetic field it develops does not change instantaneously when a step current is applied. This means that the inductance does not instantly adjust to changes in current magnitude. Therefore, it is clearer to analyse the variation of (L_M) with respect to the rotor flux linkage (ψ_{Rd}) rather than with (i_{sd}). This approach provides a more accurate interpretation of the inductance behavior. These machine parameters are initialised in the MTPA script.

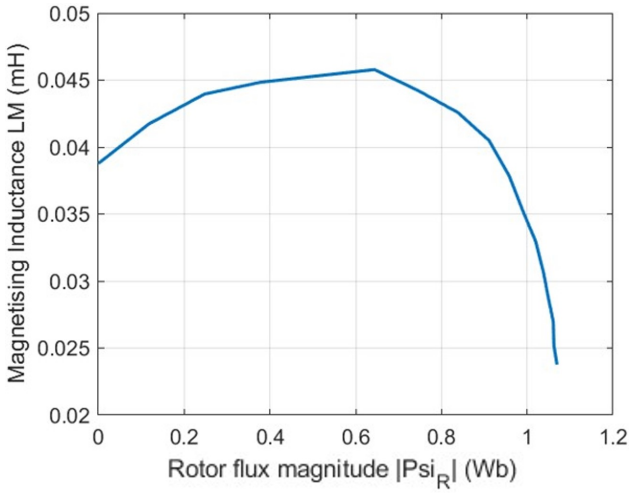

Figure 3.2: Magnetising inductance in inverse-Γ form vs Rotor Flux magnitude in inverse-Γ form

3.1.2 Solving the Optimisation problem

MATLAB's *fmincon* [10] function employs an algorithm to find the minima of the defined objective function. Typically this starts off from the initial guess of variables provided as a starting point. Further, it considers the defined non-linearities of the problem as constraints and with iterative refinement at each step the function adjusts its parameters in search of a solution that meets these constraints and eventually converges on the nearest local minimum based on the initial guess. This convergence to a local minimum is due to the nature of the optimization algorithms used by *fmincon*, which are designed to find points where the objective function value is lower than at nearby points, but not necessarily the lowest possible value across the entire feasible region.

The basic syntax of this function is

```
fmincon(fun, x0, lb, ub, nonlcon, options)
```
Where the parameters are defined as

- **fun**: A function handle to the objective function to be minimised.
- **x0**: Initial guess for the optimisation variable (currents in this case).
- **lb, ub**: Vectors defining the lower and upper bounds on the variables.
- **nonlcon**: A function handle to both the nonlinear equality and inequality constraints.
- **options**: Options for customising the optimisation such as tolerance, maximum iterations etc.

3.1.3 Rated Torque

Given that the constraints on the machine vary across different operating points, the adopted approach divides the operating region into two parts: **Constant torque region** and **Constant power region**. In the constant torque region, the machine can operate at the highest magnetic flux density without saturation. This means the machine is able to operate at its rated current which implies that it can consistently deliver rated torque. The dynamic response in this region is also great as torque output is not speed dependant. This is valid upto the rated speed of the machine.

To mathematically model this behavior to find the rated torque, the torque equation has to be maximised. Since *fmincon* is designed to minimise, the adopted approach is to take the negative of objective function. This effectively maximises the torque output. In this case, as described earlier, the only constraint is the limit on current magnitude which is handled as a non-linear equality constraint.

Following the syntax, **fun** is set to the torque equation in (2.12). An initial guess is made in the d and q direction of stator currents respectively. Since the solution is for the motoring region only, both are positive. The bounds are defined by the lower and upper current limits, making **lb, ub** equal to [0, I_{rated}] respectively. These settings must follow the constraint imposed by the current limit circle described by

(2.19). Hence, the current equation becomes the non-linear equality constraint in **nonlcon**. By executing the *fmincon* function to calculate the maximum torque under the constraint of the rated current from Table 3.1, a rated torque value of 161 Nm is obtained.

3.1.4 Rated Speed

The rated speed of the machine is the point where it produces rated torque using rated voltage, without entering field weakening. To operate the machine above its rated speed, the magnetic flux must be reduced to control the back-emf, which increases with speed. The point at which field weakening begins is referred to as the knee-point. Beyond this point, increasing speed requires field weakening. Therefore, identifying the knee point based on when the supply voltage equals the rated voltage is a practical approach to determining the rated speed.

MATLAB's *fsolve* [11] is a function specifically designed to find the roots of systems of nonlinear equations. It finds the variable values that make the function equal to zero. This solver is ideal for problems where analytical solutions are difficult to compute. It utilises numerical methods to iteratively adjust the variables until the function outputs are effectively zero. The syntax of this function is as follows

```
x = fsolve(fun, x0)
```
where

- **fun** is a function handle to the function whose solution is being solved.
- **x0** is the initial guess for the values of the solution variable.

In this application, `fsolve` is used to determine the rotor speed at which the stator voltage V_s equals the rated voltage V_{rated}. The function to be solved is $x = V_s - V_{\text{rated}}$, where V_s is calculated from the components of the stator voltage as $V_s = \sqrt{V_{sd}^2 + V_{sq}^2}$. Starting with an initial guess for the rotor speed, which is x_0, `fsolve` iteratively adjusts the rotor speed. When $x = 0$, the corresponding rotor speed is returned as the output implying that this speed is where the stator voltage is maximised without exceeding V_{rated}. For the machine used in this study, the rated speed is 650 RPM for the rated voltage in Table 3.1.

3.1.5 Field Weakening torque limit

Up to this point, the torque-speed curve has been established until the knee point, as shown in Figure 3.3. To complete the curve, all the maximum torque points from the rated speed to the maximum machine speed must be identified to cover all operating regions of the machine. This is achieved using the *fmincon* function which addresses the problem as a constrained optimisation where the objective is to maximise torque while applying constraints in the field weakening region.

The objective function **fun** is defined by the torque equation in (2.12). It is observed

that the choice of the initial guess **x0** generally does not significantly impact the solution. However, selecting a logical starting value can improve the convergence process and enhance computational efficiency. In this case, **x0** is set to [5, 5] A for both the d and q directions. The bounds **lb** and **ub** are maintained at [0, I_{rated}]. Regarding the constraints, there are two critical ones: current and voltage.

1. **Current Constraint**: This is the inequality constraint $I_{s,\text{mag}} \leq I_{s,\text{rated}}$ because at very high machine speeds, due to a large back-emf, there is insufficient voltage available to support operation at the rated current magnitude. This constraint captures the effect voltage limit dominating at high speed operation.
2. **Voltage Constraint**: Since the back-emf is directly proportional to machine speed, the voltage must not be reduced below the rated value to ensure sufficient torque production and prevent stalling. Therefore, the equality constraint $V_s = V_{rated}$ becomes necessary such that this is constantly true.

The maximum torque points extending from rated speed up to the maximum machine speed are determined by solving these equations. With this analysis, the entire torque-speed curve of the machine in the first quadrant is captured as depicted in Figure 3.3.

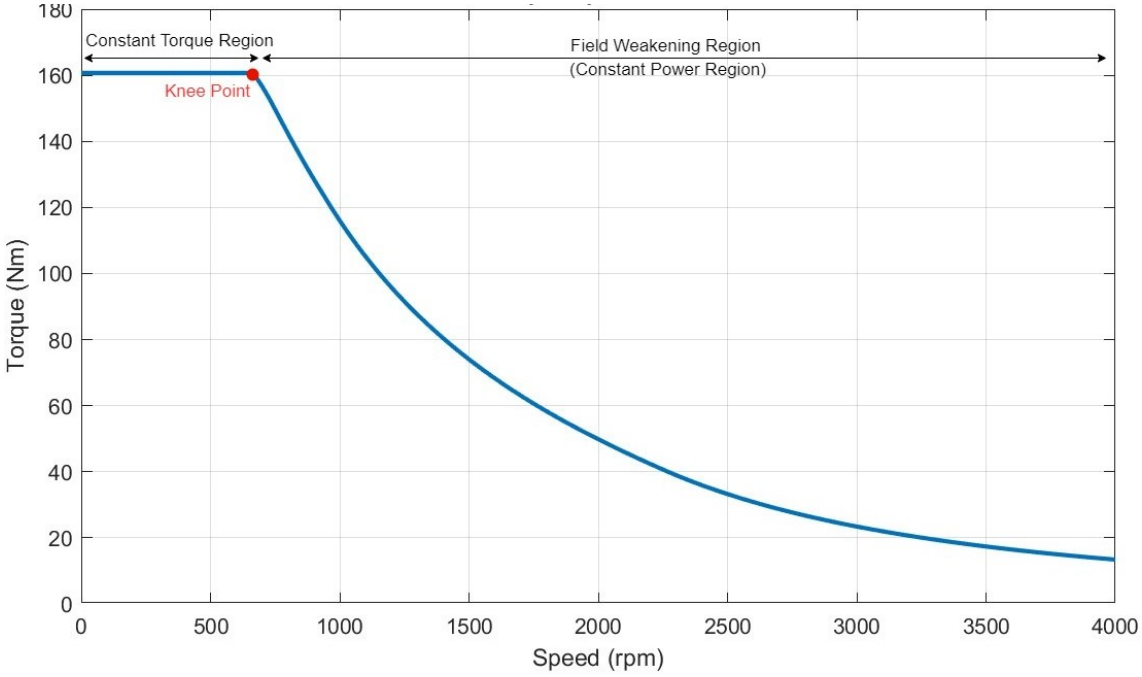

Figure 3.3: Torque Speed characteristics of the Induction Machine

3.1.6 Solving for MTPA points

The entire operating region of the machine is delineated and the next step focuses on optimising the operating points to minimise energy losses. These points are determined by minimising the current magnitude for each combination of torque and speed along the torque-speed curve. This involves solving for the conditions under which the machine uses the least amount of current to achieve the required torque at each specific speed. Minimising current not only reduces copper losses but also optimizes energy consumption, thereby improving the vehicle's range.

In the optimisation to find the MTPA points, the torque resolution is set to 1 Nm and the speed resolution to 10 RPM. By using a *for* loop, each operating point under the torque-speed curve is systematically evaluated to determine the minimum current magnitude needed to achieve them. In each iteration, which corresponds to an operating point, the algorithm calculates the minimum current magnitude required to produce the torque. The *fmincon* function is effectively used to solve this optimisation as follows:

1. A for loop to iterate through all torque values ranging from 0 to rated torque 161 Nm.

2. The objective function is to minimise the currents for the operating point being evaluated. Therefore, the stator current relation as in (2.19) is used.

3. As this optimisation is constrained, the constraints need to be specified in **nonlcon**. The constraints are as follows
   - The current magnitude should not exceed the rated current which translates to $I_{s,mag} \leq I_{rated}$.
   - The second non-linear constraint is the voltage magnitude should not exceed the maximum allowable voltage, which is $V_s \leq V_{rated}$.
   - The final condition which has to be satisfied in each solution is the torque reference, which comes from the for loop should be equal to the output torque from the torque equation. This means that the requested torque has been achieved while satisfying the other constraints in the problem.

The solution to this optimisation problem is a matrix that stores the values of i_{sd} and i_{sq}. These current reference set-point values correspond to the smallest current magnitude needed to generate the requested torque, thereby minimising Joule losses. The combinations of i_{sd} and i_{sq} when the operating points lie on the boundary of the torque-speed curve of the machine shown in Figure 3.3 are shown in Figure 3.4. The red line in Figure 3.4 represents the various combinations of i_{sd} and i_{sq} that define the machine's boundary line across the entire speed range.

The origin of the plot in Figure 3.4, located at the bottom left corner, represents the starting point where both i_{sd} and i_{sq} are 0 A. At this point, the machine is at standstill (speed is 0 rpm) and is producing 0 Nm of torque. As the machine begins to operate and both speed and torque increase, the trajectory of i_{sd} and i_{sq} follows

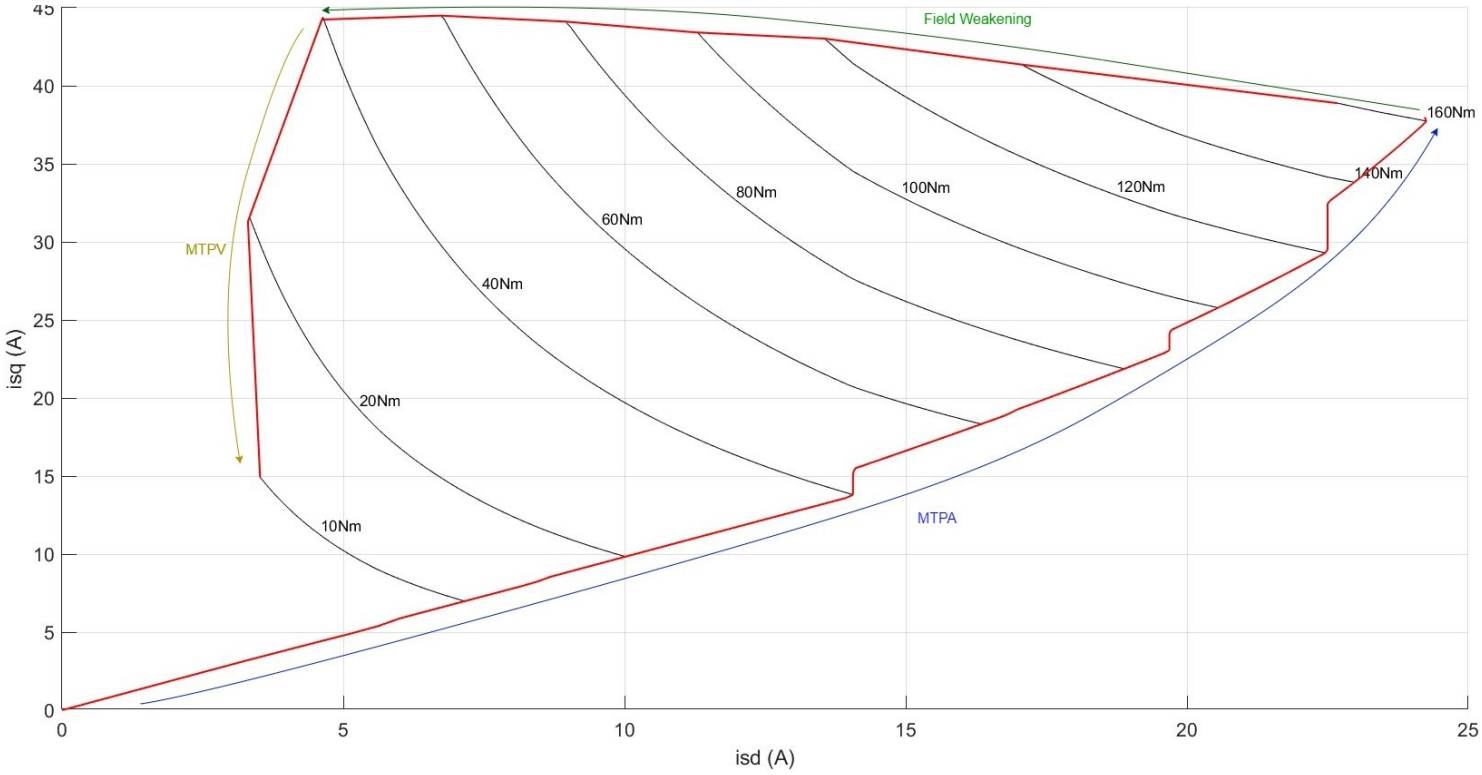

Figure 3.4: Current trajectory along the torque-speed curve boundary

the red line, moving to the right. This line shows how the current components i_{sd} and i_{sq} change for different operating conditions of the machine, specifically along the boundary where the machine operates most efficiently. The rightmost point on the red line corresponds to the machine's rated operating condition, which is fully described in Sections 3.1.3 and 3.1.4. This section of the plot also represents the Maximum Torque per Ampere (MTPA) region. Within this region, the machine is able to fully utilize both its rated current and voltage limits to achieve optimal performance, as discussed in Section 2.2.1.

As the machine's speed increases beyond the rated point, it enters the field weakening region. In this region, the machine's ability to generate maximum torque is constrained by the available voltage rather than the current. As a result, the machine can no longer maintain maximum torque because the current limit that would typically be used to generate flux and torque is now limited by the voltage, as explained in Section 2.2.2. This causes the voltage circle to shrink, as detailed in Section 2.2.2, and the transition into field weakening region is observed in Figure 3.4, where the red line begins to move left from the rated operating point. At this point, a slight increase in i_{sq} and a corresponding decrease in i_{sd} occurs and this shift happens due to the voltage circle shrinking with increasing speed, as discussed in Section 2.2.2. The machine compensates for the reduced flux by slightly increasing (i_{sq}) to meet the torque demands.

When the machine operates at very high speeds, it reaches the rated voltage limit,

meaning that its ability to produce torque at these speeds becomes constrained by this voltage limit. As explained in Section 2.2.3, this occurs because the voltage circle shrinks within the current circle, reducing the machine's capability to generate flux and torque. This operating condition is known as the Maximum Torque per Voltage (MTPV) region. In Figure 3.4, this transition into the MTPV region is illustrated by a steep decrease i_{sq} along with a decrease in i_{sd} at the leftmost part of the plot. The red line moving downward in this region represents the reduction in current values as the machine adapts to the voltage constraints and enters the MTPV region.

Tracing the red path in Figure 3.4 from the origin through the three regions of operation - MTPA, Field Weakening, and MTPV, illustrates the combinations of i_{sd} and i_{sq} that define the machine's boundary line of operation. However, if the operating point is below this boundary line, the corresponding i_{sd} and i_{sq} values will not lie on the red line. The black constant torque lines, shown in 20 Nm increments, represent the different levels of torque the machine can produce across the entire operating region. For instance, if the desired operating point is 60 Nm at a particular speed, the currents i_{sd} and i_{sq} will follow the red path until they intersect with the 60 Nm torque line. At that point, the currents would deviate from the red line and continue along the black 60 Nm line until reaching the specific operating point.

Figure 3.4 illustrates various combinations of i_{sd} and i_{sq} for operating both at the boundary curve and at points below it. These combinations are optimized to minimize the total current magnitude and Joule losses while still achieving the desired torque at a given speed. The irregular bumps and edges along the red line, rather than a smooth path, result from the way MATLAB's $fmincon$ function solves the optimization problem. As explained in Section 3.1.2, the $fmincon$ function converges to a local minimum. This can cause the solution for i_{sd} and i_{sq} at nearby operating points to converge to the same local minimum, leading to the abrupt edges and jumps visible on the red line in Figure 3.4.

3.2 Dynamic drivetrain evaluation model in Simulink

The dynamic drivetrain evaluation model in Simulink is shown in Figure 3.5. As noticed in the figure, the model consists of three main components: the induction machine, the controller and the converter. The converter is an ideal controllable voltage source that only limits the phase voltages to the rated peak phase voltage of the machine. The induction machine and controller blocks are further explained in the following chapters.

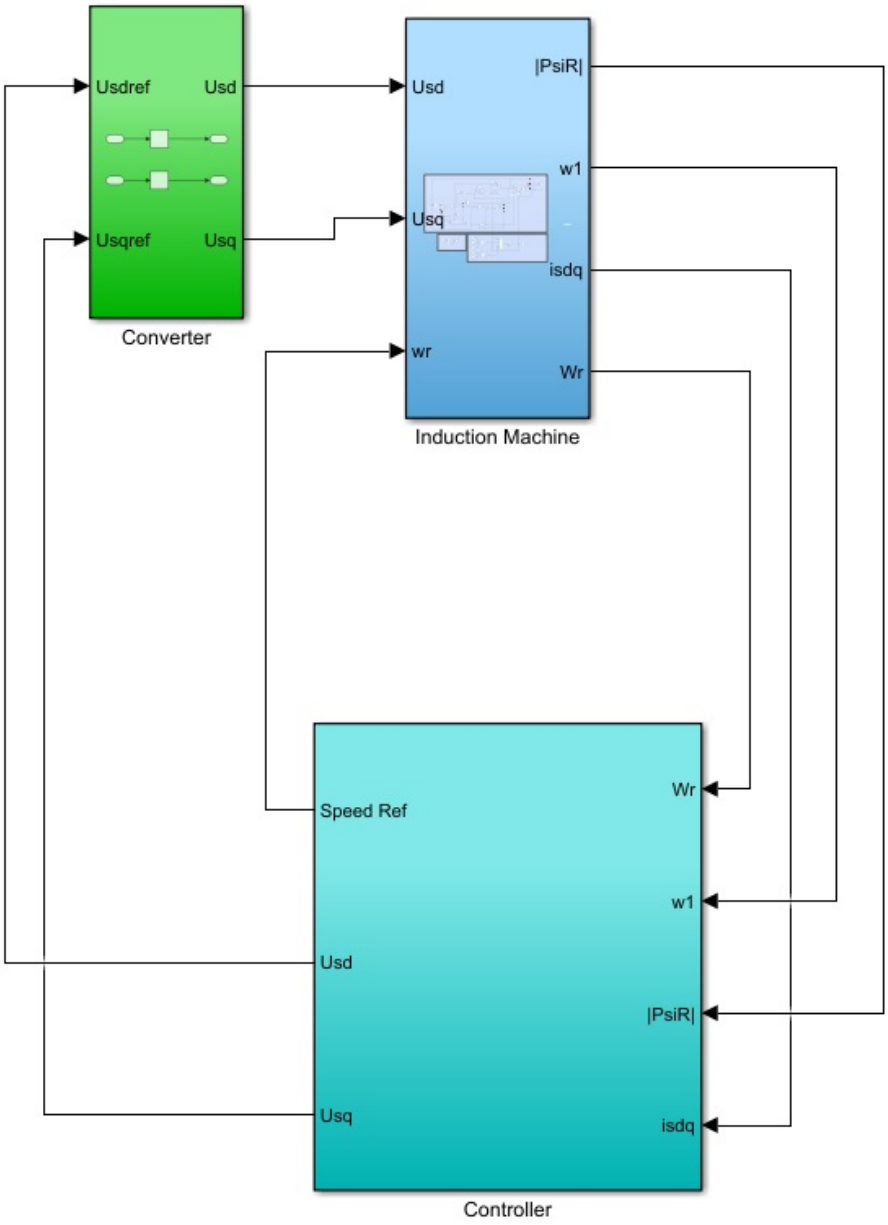

Figure 3.5: The dynamic drivetrain evaluation model in Simulink

3.2.1 Implementation of dq inverse-Γ model

The inverse-Γ model in the *dq* reference frame is used for implementing the induction machine block in Figure 3.5. This approach ensures consistency with the MTPA calculations and the control system, both of which are based on this model. Additionally, this model accounts for the saturation effects of the magnetising inductance, as illustrated in Figure 3.2. The three-phase stator voltage input is transformed into *dq* using the Clarke and Park transformations and the angle of the rotor flux linkage. To model the current dynamics, (2.9) and (2.10) are written on state space form as

$$\frac{di_{sd}}{dt} = \frac{v_{sd} - (R_s + R_R)i_{sd} + \frac{R_R}{L_M}\psi_{Rd} + \omega_1 L_\sigma i_{sq}}{L_\sigma} \tag{3.7}$$

and

$$\frac{di_{sq}}{dt} = \frac{v_{sq} - (R_s + R_R)i_{sq} - \omega_r \psi_{Rq} - \omega_1 L_\sigma i_{sd}}{L_\sigma} \tag{3.8}$$

The *dq* currents in the machine are obtained by integrating (3.7) and (3.8) and the implementation in Simulink is shown in Figure 3.6.

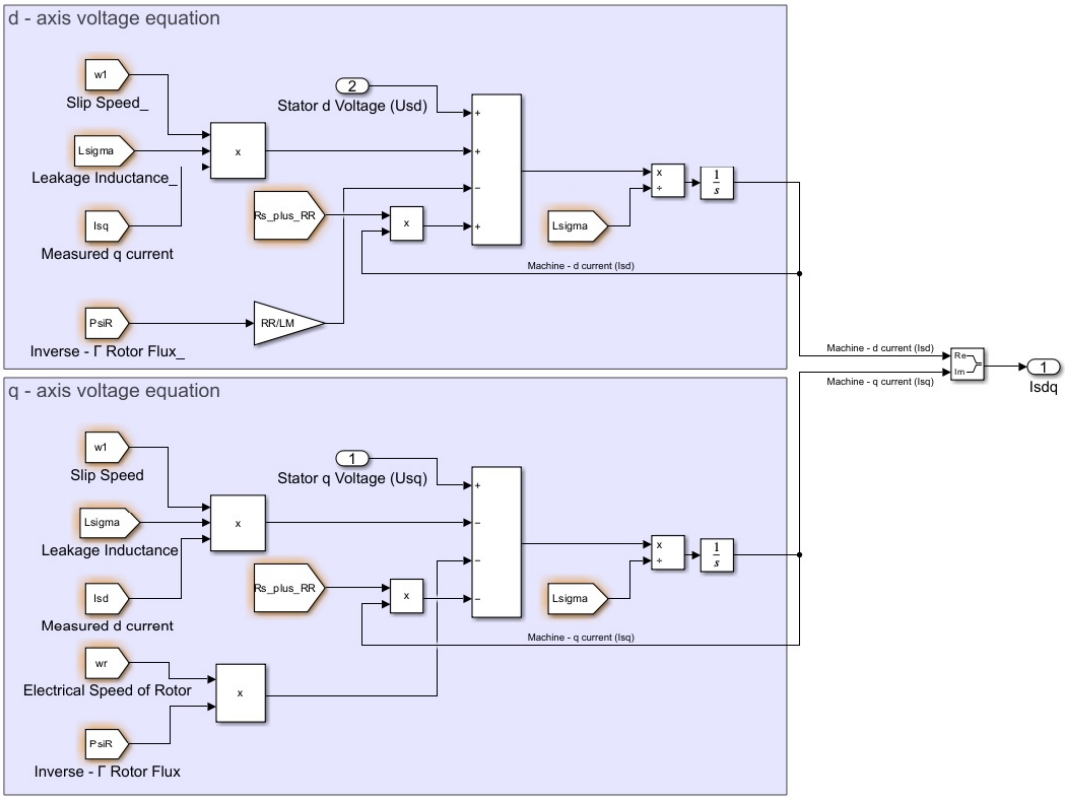

Figure 3.6: IM model in inverse-Γ dq form

The rotor flux for the inverse-Γ model is described with (2.6) and if the d-axis is aligned with the rotor flux linkage, the real part of the equation becomes (2.11).

This equation is repeated here for simplicity

$$\frac{d\psi_{Rd}}{dt} = R_R i_{sd} - \frac{R_R}{L_M(\psi_{Rd})}\psi_{Rd} \tag{3.9}$$

In (3.9) which represents the flux dynamics, the magnetising inductance is a function of the rotor flux magnitude (d-component since the flux is aligned in the d-direction). The rotor flux magnitude is obtained by integrating (3.9) and this is implemented in Simulink as shown in Figure 3.7. The lookup table for L_M in the figure is according to Figure 3.2.

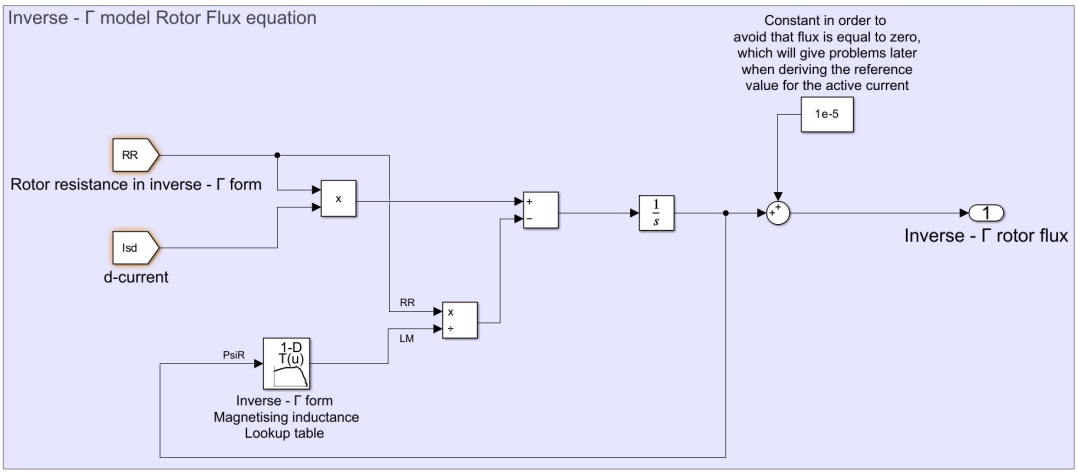

Figure 3.7: Inverse-Γ form flux equation modelling in Simulink

The torque produced in the machine is calculated by (2.12), and the implementation in Simulink is as shown in Figure 3.8.

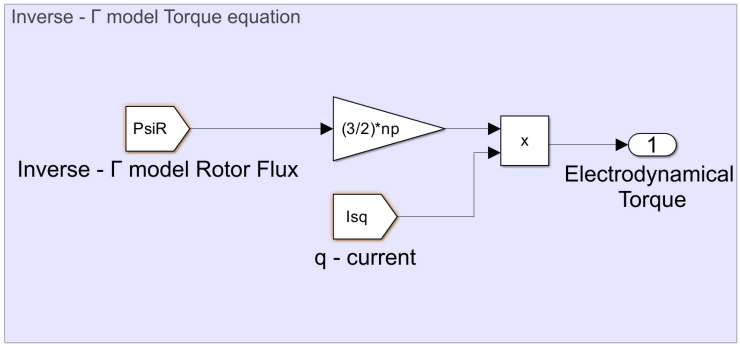

Figure 3.8: Inverse-Γ form torque equation modelling in Simulink

The machine's inertia introduced an additional degree of freedom, complicating computations and making it difficult to set the machine's speed. This often caused simulation crashes or resulted in the simulation exceeding the machine bounds due to rapid acceleration or complicating the calculation of derivatives. To address these issues, the mechanical model of the drivetrain was removed and the mechanical inertia of the drivetrain (vehicle) was assumed to be very large. This assumption means that

any change in speed over time is negligible because the large inertia causes speed changes to occur very slowly. By making this simplification, the model becomes more manageable and avoids going out of bounds during simulations. Therefore, to align with the scope of the thesis and effectively observe the machine's behavior, it was determined that focusing solely on the electrodynamic torque of the induction machine is sufficient. This decision is based on the assumption made about the mechanical inertia of the drivetrain. Due to the removal of the mechanical model, the speed of the machine was modeled as an input and in the control system block this speed is set according to the wanted operating point, as can be seen in Figure 3.5.

The stator frequency is modeled using the slip equation for an induction machine,

$$\omega_1 - \omega_r = \frac{R_R i_{sq}}{L_M i_{sd}} \tag{3.10}$$

Equation (3.10) can be re written as,

$$\omega_1 - \omega_r = \frac{R_R i_{sq}}{\psi_{Rd}} \tag{3.11}$$

In (3.11), the term ω_r is transposed to the right-hand side of the equation to express the stator frequency ω_1 as the sum of ω_r and the remaining term, resulting in (3.12). The corresponding model is implemented in Simulink, as illustrated in Figure 3.9.

$$\omega_1 = \omega_r + \frac{R_R i_{sq}}{\psi_{Rd}} \tag{3.12}$$

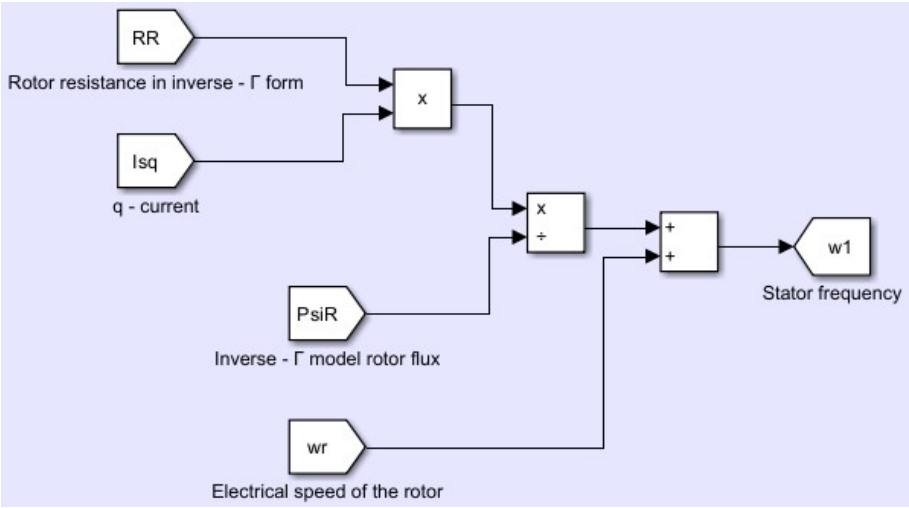

Figure 3.9: Stator frequency equation modelling in Simulink

3.2.2 Controller

Various vector control strategies have been developed to enhance performance and simplify the implementation of electric machines. One of these strategies is Field

Oriented Control (FOC). It works by decoupling the machine's torque and magnetic flux components through Park and Clark transformations, allowing for independent control of each component. This method simplifies a complex machine model into two individually controllable currents: the torque producing current (i_{sq}) and the flux producing current (i_{sd}). The advantages of this method include a smooth response to changes, good performance in both transient and steady-state conditions, and easily adjustable parameters for controlling different machines [12]. However, the drawback is that it relies on perfect field orientation, making it sensitive to parameter estimation errors such as inaccuracies in rotor angle. But it is commonly used in most electric vehicles today due to its overall benefits [2]. This work does not focus on the optimal control of dq-currents. Instead, it examines how to adjust dq-current references to achieve smooth transitions between different operating points of the drivetrain. The Field-Oriented Control (FOC) method is utilized because it is commonly used and effective in controlling the currents in the machine.

The controller block in Figure 3.5 consists of several blocks: current controller, current reference calculation, and a speed controller. The calculation of the current references is described in the next section. The current controller within the control system remains unchanged from the original model designed as part of the EEN140 course curriculum. It employs a PI (Proportional-Integral) controller, which primarily utilizes the discrepancy between the measured dq-current from the machine and the reference currents. Along with this, an anti-windup term, a cross-coupling term, and a feedforward term are used to generate the reference dq-voltage for the machine. The reference dq-voltage is sent to the machine as can be seen in Figure 3.5. A Simulink representation of the current controller is shown in Figure 3.10. The closed-loop transfer function is shaped to be a first-order low-pass filter with gain one [13] and with a bandwidth $\alpha_c = 1600\,\text{rad/s}$. This gives that the controller gains are calculated as:

$$K_{p,c} \approx 7.5$$

$$K_{i,c} \approx 11917$$

The added active damping is selected so that the modified process model gets the same bandwidth as the closed loop system [13], this gives,

$$R_a = 7.1012$$

The anti-windup function is tuned to give a tracking time constant of the integrator equal to the closed-loop system time constant [13], which means that the gain Antiwindup in Figure 3.10 is $\frac{1}{K_{p,c}}$.

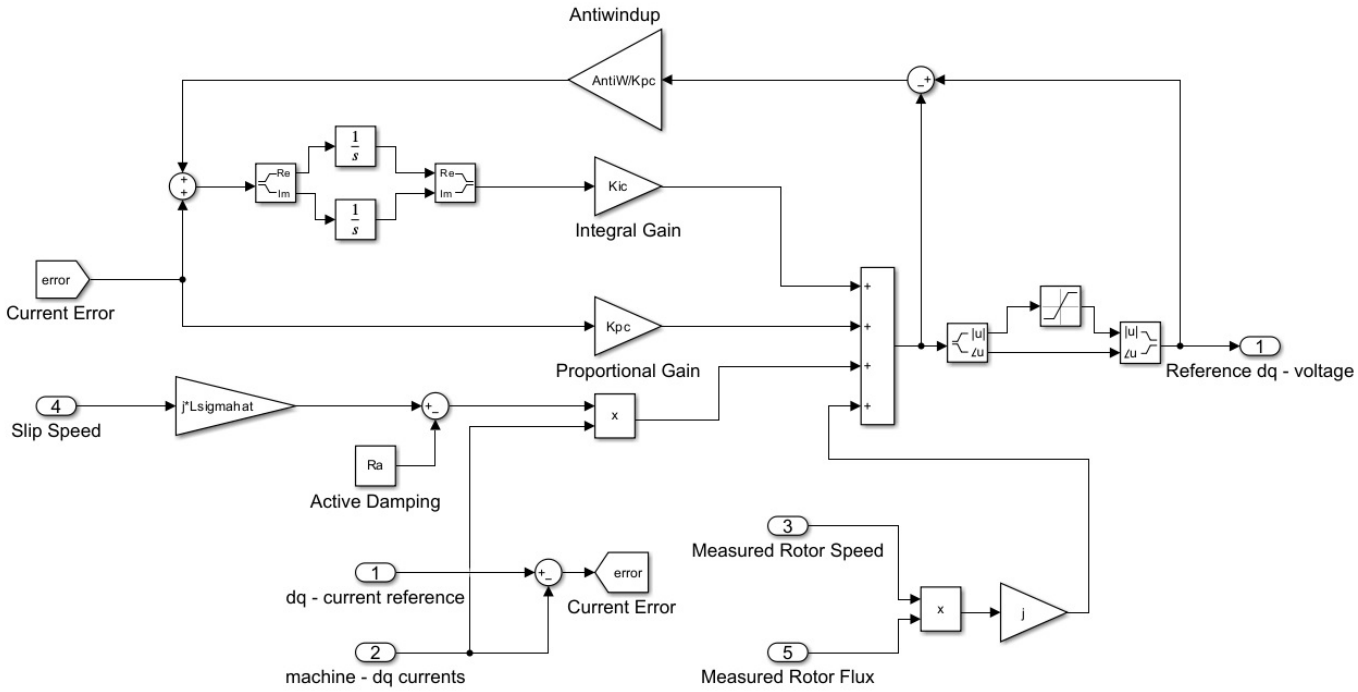

Figure 3.10: Simulink implementation of the current controller

The speed control is intentionally simplified to focus on studying the current control strategies during transients. Excluding the mechanical dynamics creates a more controlled environment to investigate how different control strategies impact the machine's electrical behavior while omitting its mechanical behavior. This setup is analogous to a machine under examination in a dynamometer setup where the speed is kept constant while torque changes are explored. A representation of this concept in Simulink is shown in Figure 3.11, where an Integrator controller is used to smoothly change the speed of the machine.

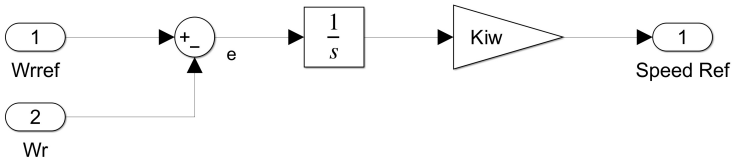

Figure 3.11: Simulink implementation of the speed controller

3.2.3 Current Reference calculations

The current reference calculation system within the machine model's control system is shown in Figure 3.12 and it computes the magnetising (i_{sd}) and torque-producing (i_{sq}) currents based on the MTPA points derived earlier. In Simulink, the 2D lookup

table function is used, whose inputs are the machine speed and torque reference. The 2D lookup table interpolates to determine the reference current values, which are used to generate the torque request at a given speed.

Additionally, a lookup table for magnetizing inductance in the inverse-Γ form (L_M) is implemented within the current reference calculation block. This setup allows for the generation of the required flux reference ($\psi_{R,ref}$) needed to produce the requested torque at a given speed. This is achieved by incorporating a 1D lookup table for L_M which varies based on the MTPA i_{sd} value corresponding to the desired torque and speed of the machine. The reference magnetizing current ($i_{sd,ref}$) is then multiplied by L_M to generate $\psi_{R,ref}$, as illustrated in Figure 3.12.

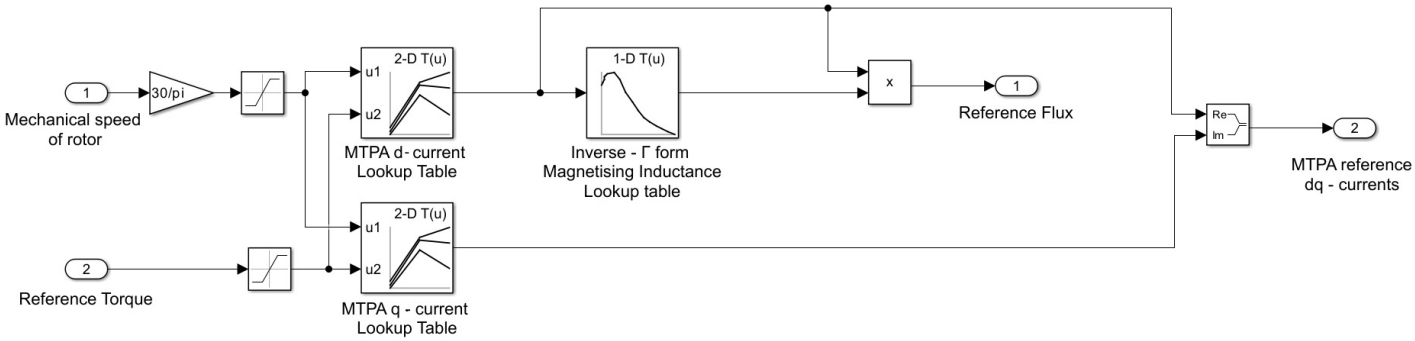

Figure 3.12: Simulink implementation of Current reference calculating system

3.3 Limitations in the dynamic response of the controller

When the MTPA current trajectory is followed during transients, it results in a slow dynamic response of the drivetrain. This is illustrated in Figure 3.13 (b), where the drivetrain starts from standstill and the torque reference ramps up to 100 Nm at 0.1s, as shown in subplot (b). In subplot (a), it can be seen that the flux reference increases with the torque reference. The increase in flux is quite slow compared to the reference, which is expected because the rotor flux dynamics are not controlled. The speed at which the rotor flux changes is determined by the time constant of the rotor flux in the machine. This time constant is

$$\tau_{\psi_R} = \frac{L_M}{R_R} \tag{3.13}$$

and at rated flux in the machine it is,

$$\tau_{\psi_{R,rated}} = \frac{0.0388H}{0.1631\Omega} = 0.2378s$$

The slow response in the buildup of the rotor flux also results in a slow response in torque, as seen in Figure 3.13(b). This type of performance in achieving the torque reference is undesirable for the driver in automotive applications, where meeting the torque reference quickly is crucial. While operating at the MTPA points is highly efficient in steady-state conditions, it is observed that following the MTPA trajectory does not ensure a dynamic transient response. The transient response is particularly important because it determines the responsiveness and dynamic capabilities of the drive system.

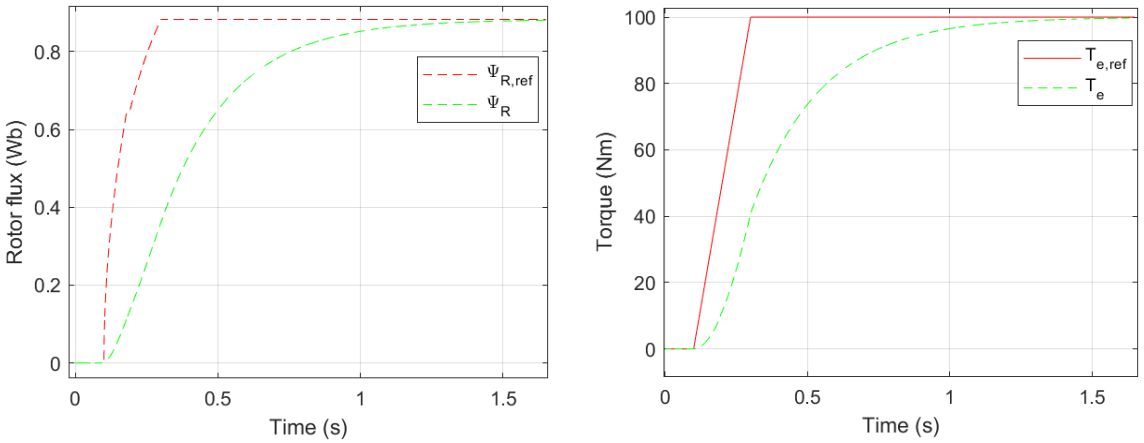

(a) Flux response

(b) Torque response

Figure 3.13: Responses in Flux and Torque while following MTPA current trajectory

As seen in Figure 3.13, relying solely on following the MTPA currents trajectory reveals a limitation in the form of responsiveness and time taken to reach the steady state operating point. This limitation becomes significant in scenarios requiring quick changes in operating conditions, such as, overtaking or quick acceleration from standstill. To address this a dynamic control strategy is needed, whose main goal is ensuring that the drivetrain can respond promptly to changes in torque demand, thus improving the dynamics of the drive system. This is further explored in Chapter 4.

4

Flux and Torque Control

This chapter explores methods to address the challenges faced in Chapter 3 when operating the machine along the MTPA trajectory. Strategies for actively controlling i_{sd} and the i_{sq} are described and their performances are demonstrated. Additionally, the trade-offs and the practicalities associated with these control methods are highlighted.

4.1 Active Flux control

From a driveability perspective, achieving a quick torque response is crucial. As discussed in Section 3.3, improving drivetrain responsiveness requires achieving the desired torque in the shortest possible time. The torque equation in (2.12) indicates that there are two variables that can be controlled to achieve the required torque: the magnetic flux (ψ_R) or the torque producing current component (i_{sq}). However, in an induction machine, the magnetic flux has to be induced to generate electromagnetic torque. Consequently, when a torque request $T_{e,\text{ref}}$ is made, at steady-state both i_{sq} and i_{sq} must settle on the MTPA trajectory for the best efficiency. But for an instantaneous torque response, it is evident from Section 3.3 that either i_{sd}, i_{sq}, or both must be boosted during the transient period. Once the flux reaches a steady-state, the currents can be adjusted back to their MTPA trajectories for minimum losses.

To address the transition between two steady-state points, introducing a flux controller improves the machine performance by actively controlling i_{sd} to generate flux more quickly. This quick path to a steady-state in flux is beneficial because it enhances the machine's responsiveness to torque changes and makes it agile during transients. However, this method induces a temporary deviation from the MTPA trajectory in i_{sd}. A Proportional-Integral (PI) controller is particularly useful in the transients as there is an error between the reference flux and the actual machine flux as seen in Figure 3.13 (a), which is $\psi_{error} = \psi_{ref} - \psi_R$. A PI controller will continuously minimise the ψ_{error}, ensuring that the desired flux is achieved quickly. This active control strategy allows for a faster and more precise adjustment of the flux, thereby improving the overall driveability.

4.1.1 Active Flux Controller Implementation

The flux dynamics in the induction machine is described by (3.9) and this is used to describe the plant transfer function, which describes the relationship between input i_{sd} and output ψ_{Rd} of the process that is controlled. When designing the flux controller the current controller is assumed to be much faster so it can be assumed that the actual d-current is equal to the d-current reference. The closed loop system for the flux controller is shown in Figure 4.1 The closed loop transfer function is shaped to be a first order low-pass filter with gain one [13] and with a bandwidth $\alpha_\psi = 400\,\text{rad/s}$. This gives that the controller gains are calculated as :

$$K_{p,\psi} \approx 2453$$
$$K_{i,\psi} \approx 12926$$

The anti-windup function is tuned to give a tracking time constant of the integrator equal to the closed loop system time constant [13], which gives that the gain Antiwindup in Figure 4.1 is $\frac{1}{K_{p,\psi}}$.

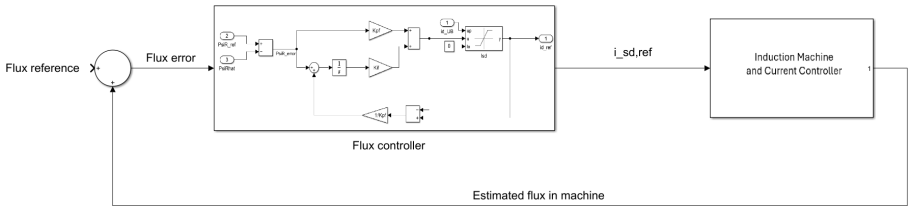

Figure 4.1: Active Flux Control working principle

4.1.2 Controller Performance

In this section the performance of the drivetrain with the active flux controller is investigated. The same references as was used in Figure 3.13 are used for this investigation. This means that the drivetrain is started from standstill and the torque reference is ramped up to 100 Nm at 0.1 s, as can be seen in Figure 4.2 (b). In subplot (a) it can be noticed how the flux reference increases with the torque reference. In Figure 4.2 (a) it is clearly noted that the machine flux ψ_{Rd} reaches its steady state value with a time of about 0.25 s as compared to 1.5 s without flux control which is seen in Figure 3.13 (a). A similar trend is observed with the torque, which in Figure 4.2 (b) settles to the steady-state value in a shorter time, compared to Figure 3.13 (b).

To be able to reduce the time taken to magnetise the machine, i_{sd} has to be increased beyond the MTPA value, as seen in Figure 4.2 (c) where it can be observed that i_{sd} is boosted between 0.1 s and 0.3 s after which it settles back on to the MTPA trajectory. This is the time frame within which the flux reaches to its new steady state value. In this way, the limitation of flux build-up as seen in Figure 3.13 (a) is overcome. Once this new steady state flux is reached, the machine has better responsiveness to torque changes.

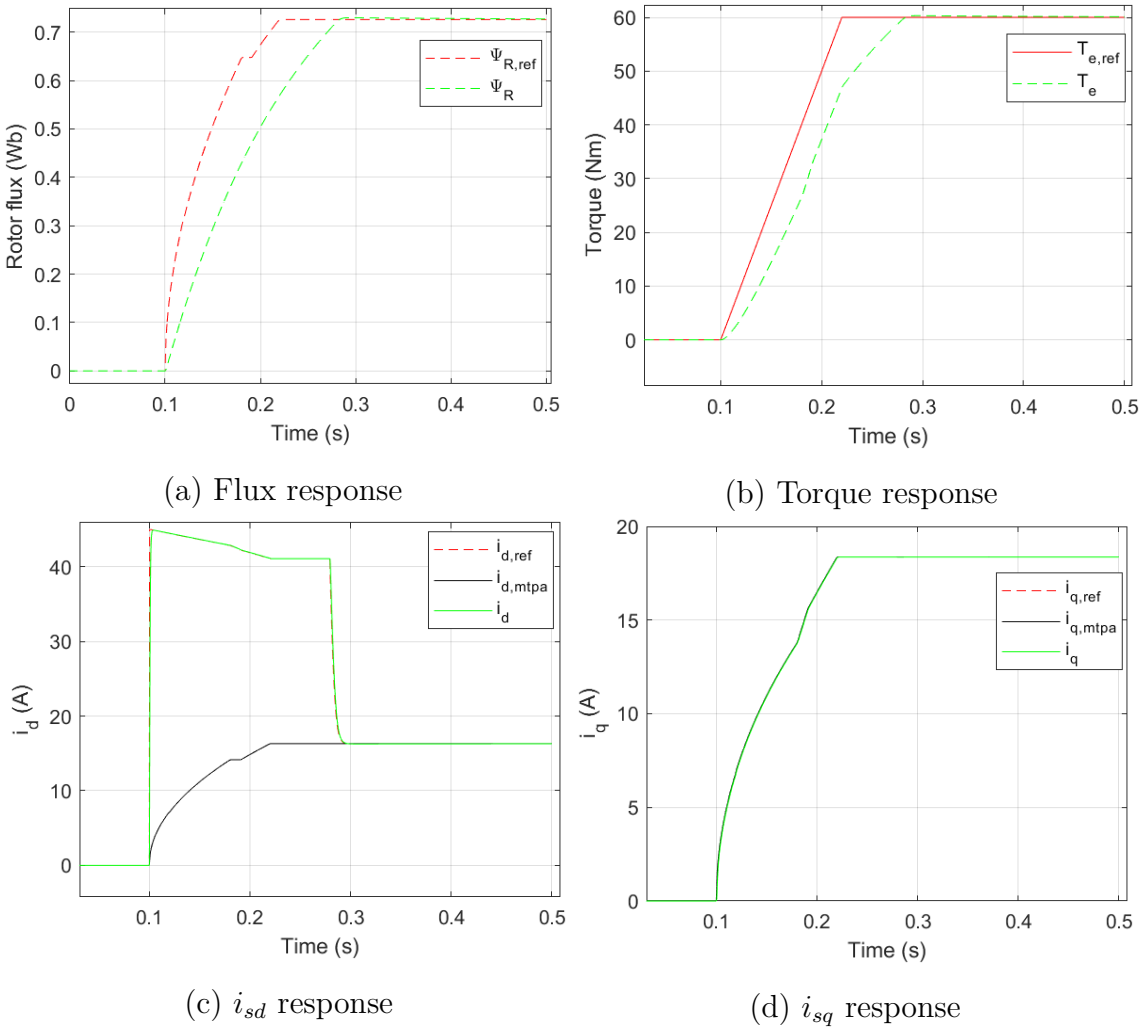

(a) Flux response

(b) Torque response

(c) i_{sd} response

(d) i_{sq} response

Figure 4.2: Machine response with Flux controller

Practical implementation:

- This temporary deviation in i_{sd} from the MTPA trajectory means that this path results in more Joule losses due to the increased current magnitude. However, this control works to reduce the rise time for flux in the machine which helps to produce torque quicker.

- The performance of this flux controller when the drive system is subjected to various control strategies are presented in Chapter 5.

Despite actively controlling the flux, it is observed from Figure 4.2 (a) that ψ_R does not exactly track $\psi_{R,ref}$. This ψ_{error} induces a lag in torque production when i_{sq} follows $i_{sq,MTPA}$. To achieve an instantaneous torque tracking, an additional contribution is needed by boosting i_{sq}, ensuring that T_e equals $T_{e,ref}$ and this contribution is discussed in the next section.

4.2 Torque current control

Active flux control enables the flux to reach its new steady state more quickly. However, the torque still lags behind its reference, as shown in Figure 4.2 (b). This lag is especially noticeable during high acceleration rates or large torque ramps. The reason for this is the controller bandwidth and the maximum d-current available in the current magnitude, which determine how quickly the flux can be changed in the machine. Thus, ψ_R does not perfectly follow its reference $\psi_{R,ref}$. If i_{sq} follows the MTPA trajectory during this time, naturally the torque will not follow the reference accurately due to the presence of ψ_{error}. To align the actual torque T_e with its reference $T_{e,ref}$, there needs to be an additional boost in i_{sq} until the flux reaches the MTPA flux level. This approach could be useful in situations where performance is prioritised, and its performance in Figure 4.3 (b) clearly shows that the previous lag has been overcome. In Figure 4.3 the same references as in Figure 3.13 and Figure 4.2 are used.

The procedure to determine this extra i_{sq} is derived from (2.12). When $T_e = T_{e,ref}$ and the equation is transposed to solve for i_{sq}, it gives the necessary compensation to achieve instantaneous torque tracking.

$$i_{sq} = \frac{T_{e,ref}}{1.5 n_p \psi_{Rd}} \tag{4.1}$$

where ψ_{Rd} is the available magnetisation in the machine.

This relation determines the compensation factor needed in i_{sq} to meet the torque requirement with the presence of ψ_{error}. Upon the flux reaching steady-state, i_{sq} is adjusted to follow the MTPA trajectory, but before this the i_{sq} is boosted to meet the torque reference with the available flux. This can be seen in Figure 4.3 (d).

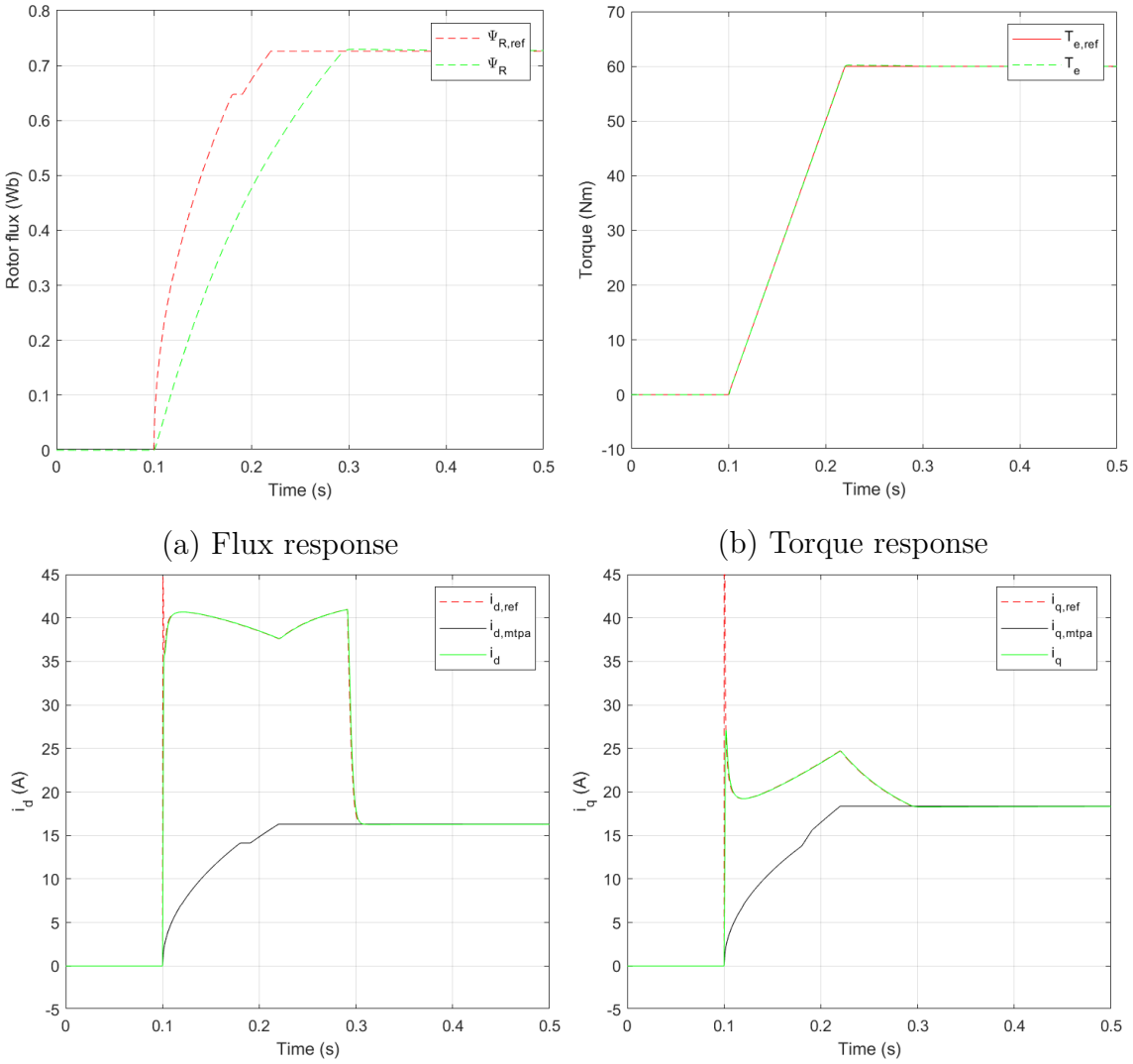

(a) Flux response

(b) Torque response

(c) i_{sd} response

(d) i_{sq} response

Figure 4.3: Machine response with i_{sq} boost

Practical implementation:

- Since this compensation term deviates i_{sq} from its MTPA trajectory, this path taken has more Joule losses. However, this is only until the flux reaches its new steady state making it highly beneficial during high torque demands in low speed regions.

- Magnetic flux density is an estimated value and not directly measurable which makes it prone to estimation inaccuracies. Consequently, in this method there is a risk of overestimation or underestimation of i_{sq} which can affect the accuracy of the control strategy.

- This strategy naturally has an increased current consumption but ensures the quickest rise time for meeting the torque demand. Hence, it is suitable to employ in scenarios where performance is prioritised over energy consumption.

5
Results and Discussions

The strategies discussed in Chapter 4 are tested at various operating points and conditions such as the constant torque and field weakening regions. This chapter examines how the different strategies perform under these conditions and evaluates their respective trade-offs.

5.1 Constant Torque region

The machine is brought to a steady state operating point of 70 Nm at 500 RPM which is a point in the constant torque region, as can be seen in Figure 5.1. Once it settles here, the machine behaviour for small torque request increase of 20 Nm is studied for three different control strategies:

- **Strategy 1:** Active flux control is enabled, and i_{sq} follows the MTPA trajectory. In this strategy the current magnitude is split such that the current magnitude required for i_{sq} to follow it's MTPA trajectory is reserved and the remaining current magnitude, up to rated current, is allowed to be utilised fully to boost i_{sd}.

- **Strategy 2:** Both Active flux control and torque current control are enabled. This allows both current components i_{sd} and i_{sq} to deviate from their MTPA trajectories until the flux reaches its steady-state reference value while meeting the reqested torque. In this strategy the current magnitude is split such that the current magnitude required for i_{sd} to follow it's MTPA trajectory is reserved and the remaining current magnitude, up to rated current, is allowed to be utilised for boosting both currents i_{sd} and i_{sq}.

- **Strategy 3:** i_{sd} follows the MTPA trajectory, while torque current control is enabled for i_{sq}. In this strategy the current magnitude is split such that the current magnitude required for i_{sd} to follow it's MTPA trajectory is reserved and the remaining current magnitude, up to rated current, is allowed to be utilised fully to boost i_{sq}.

The above strategies are analysed for various operating points and are discussed further using Figures 5.1, 5.2 and 5.3 respectively. The observations for each strategy are summarised as follows:

Strategy 1: The rise in flux is very quick, as observed in Figure 5.1(a) due to the deviation of i_{sd} away from it's MTPA trajectory when required for a short period of time before settling back to it's MTPA value, as seen in Figure 5.1(c). There is only a small deviation in the actual torque from the torque request during the first torque ramp due to that the flux does not rise as quick as the reference, but otherwise (for the second small torque ramp) the torque request is met perfectly as shown in Figure 5.1(b). The results for the energy losses, stator power, shaft power and power losses for **Strategy 1** for torque request increase of 20 Nm are shown in Table 5.1. The stator and shaft powers are given after the torque request increase, for the final value in Figure 5.1. The energy loss is the power losses, stator power subtracted with shaft power, integrated from 0s to 3.5s.

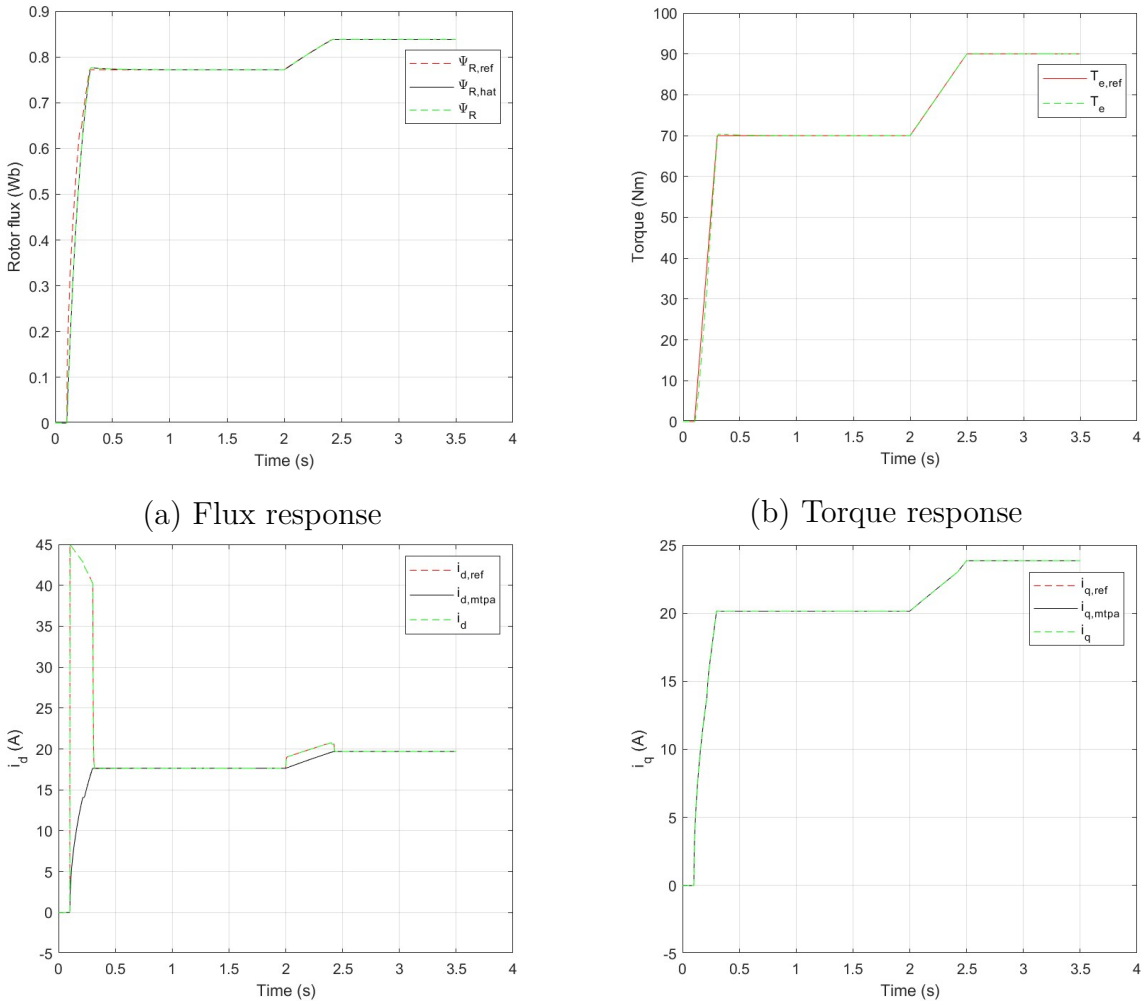

(a) Flux response

(b) Torque response

(c) i_{sd} response

(d) i_{sq} response

Figure 5.1: Machine and current response for Strategy 1

Table 5.1: Results data for torque request increase of 20 Nm for Strategy 1

Torque request increase from 70 Nm to 90 Nm	Strategy - 1			
	Energy losses (kJ)	Stator Power (kW)	Shaft Power (kW)	Power Losses (%)
	0.984	5.11	4.71	7.82

Strategy 2: The flux rises quickly as illustrated in Figure 5.2(a), though not as fast as in Strategy 1 since the available portion of the current magnitude for i_{sd} to deviate from its MTPA trajectory is lesser than Strategy 1 as torque control is enabled and this is reflected in Figure 5.2(c). The torque request is followed perfectly (both for the large and the small torque request ramp) as indicated by the green line T_e shown in Figure 5.2(b). The results for the energy losses, stator power, shaft power and power losses for **Strategy 2** for torque request increase of 20 Nm are shown in Table 5.2. The stator and shaft powers are given after the torque request increase, for the final value in Figure 5.2. The energy loss is the power losses, stator power subtracted with shaft power, integrated from 0s to 3.5s.

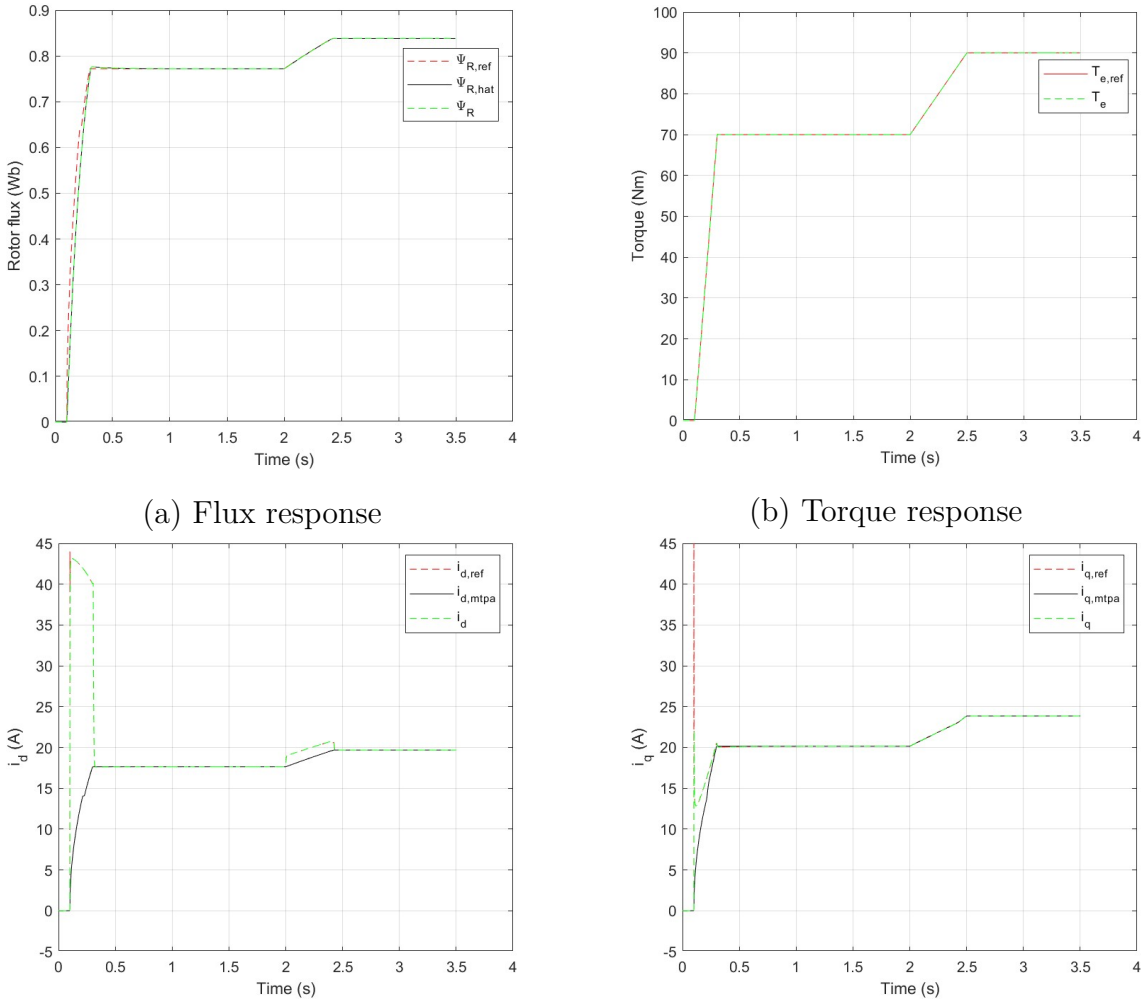

(a) Flux response

(b) Torque response

(c) i_{sd} response

(d) i_{sq} response

Figure 5.2: Machine and current response for Strategy 2

Table 5.2: Results data for torque request increase of 20 Nm for Strategy 2

Torque request increase from 70 Nm to 90 Nm	Strategy - 2			
	Energy losses (kJ)	Stator Power (kW)	Shaft Power (kW)	Power Losses (%)
	0.984	**5.11**	**4.71**	**7.82**

Strategy 3: The flux takes a longer time to achieve a steady state because flux control is not enabled as shown in Figure 5.3(a). However, the torque request for the first ramp is not met perfectly due to the lower level of flux present in the machine, as a large portion of the current magnitude is being used to boost i_{sq} to meet the torque request and therefore i_{sd} is limited due to this. The torque request profile is as shown in Figure 5.3(b). The results for the energy losses, stator power, shaft power and power losses for **Strategy 3** for torque request increase of 20 Nm are are shown in Table 5.3. The stator and shaft powers are given after the torque request increase, for the final value in Figure 5.3. The energy loss is the power losses, stator power subtracted with shaft power, integrated from 0s to 3.5 s.

This strategy, however, is not going to be considered for future test cases since it always consumes the most energy due to the utilization of the maximum value of current magnitude for the longest duration among the 3 strategies. This utilization of current magnitude can be observed in Figure 5.3(d), where i_{sq} has to be boosted for a much longer duration above it's MTPA trajectory to meet the torque request in Figure 5.3(b) as the flux present in the machine is lower than the required amount as observed in Figure 5.3(a) due to i_{sd} following its MTPA trajectory as observed in Figure 5.3(c).

The spike in i_{sd} at 0.1s in Figure 5.3(c) occurs due to reaching the voltage limit, resulting in a loss of control over both i_{sd} and i_{sq}. To prevent this deviation and keep i_{sd} following its MTPA trajectory in this strategy, a significant amount of negative d-voltage would need to be applied. However, this is not feasible without a separate voltage limiter that prioritizes d-voltage over q-voltage, which would prevent the overshoot in i_{sd} as seen in Figure 5.3(c). The downside of prioritizing d-voltage is that it increases the time needed to boost the q-current because the available voltage for controlling i_{sq} is reduced compared to the scenario where d-voltage is not prioritized.

Table 5.3: Results data for torque request increase of 20 Nm for Strategy 3

Torque request increase from 70 Nm to 90 Nm	Strategy - 3			
	Energy losses (kJ)	Stator Power (kW)	Shaft Power (kW)	Power Losses (%)
	1.13	**5.11**	**4.71**	**7.82**

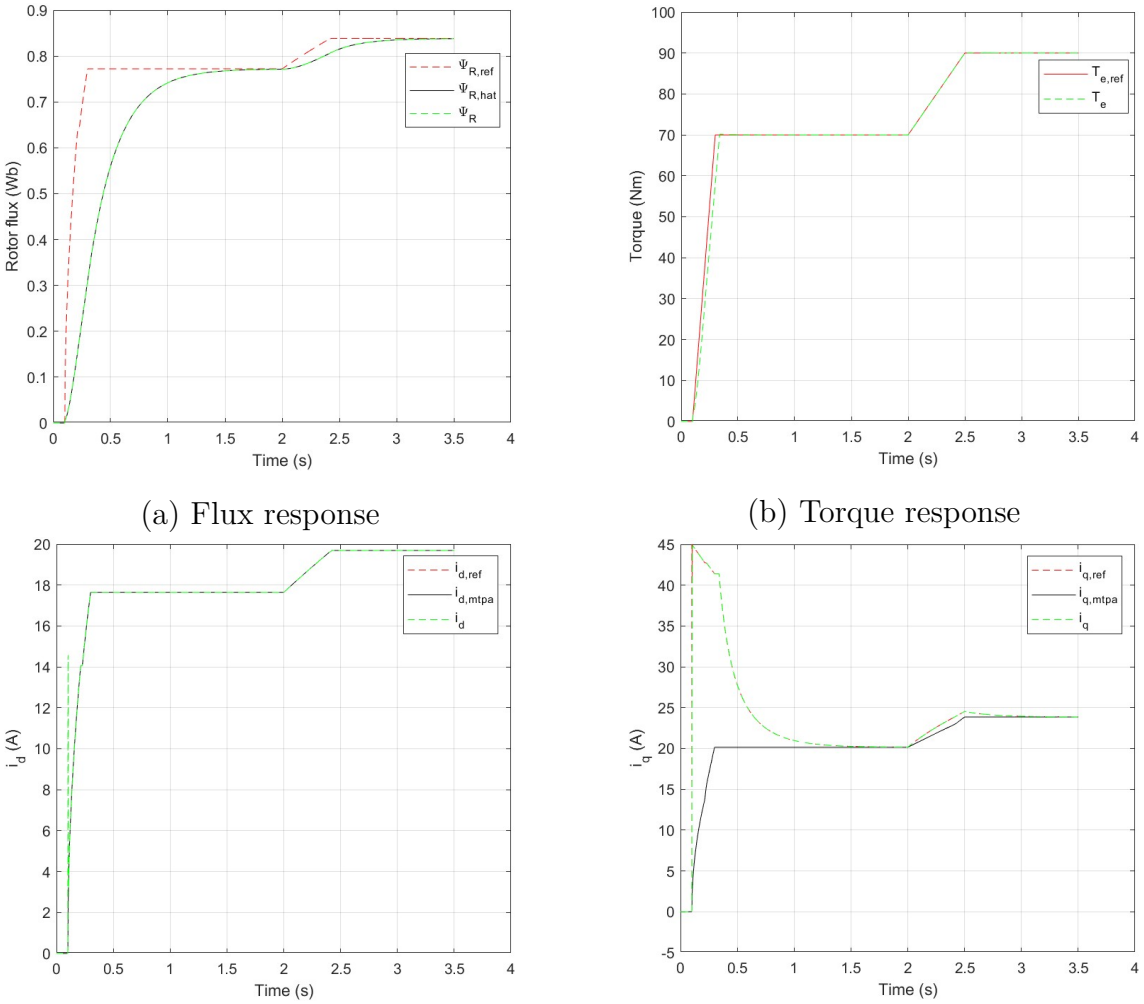

(a) Flux response

(b) Torque response

(c) i_{sd} response

(d) i_{sq} response

Figure 5.3: Machine and current response for Strategy 3

The downtrend response is also tested for this test case and for Strategy 1, where the torque request is ramped down from the steady state operating point of 70 Nm to a value of 50 Nm, which in turn means there is a flux reduction with respect to time. The results for this case is shown in Figure 5.4. As can be seen in Figure 5.4(b), the torque follows the request during the ramp down. This is due to that the ramp is slow so that the active flux controller is able to keep the flux equal to the flux reference during the ramp down. Since reducing the flux means a lower d-current there is no current limiter active in this case. The results for the energy losses, stator power, shaft power and power losses for Strategy 1 for torque request decrease of 20 Nm are shown in Table 5.4. The stator and shaft powers are given after the torque request increase, for the final value in Figure 5.4. The energy loss is the power losses, stator power subtracted with shaft power, integrated from 0s to 3.5 s.

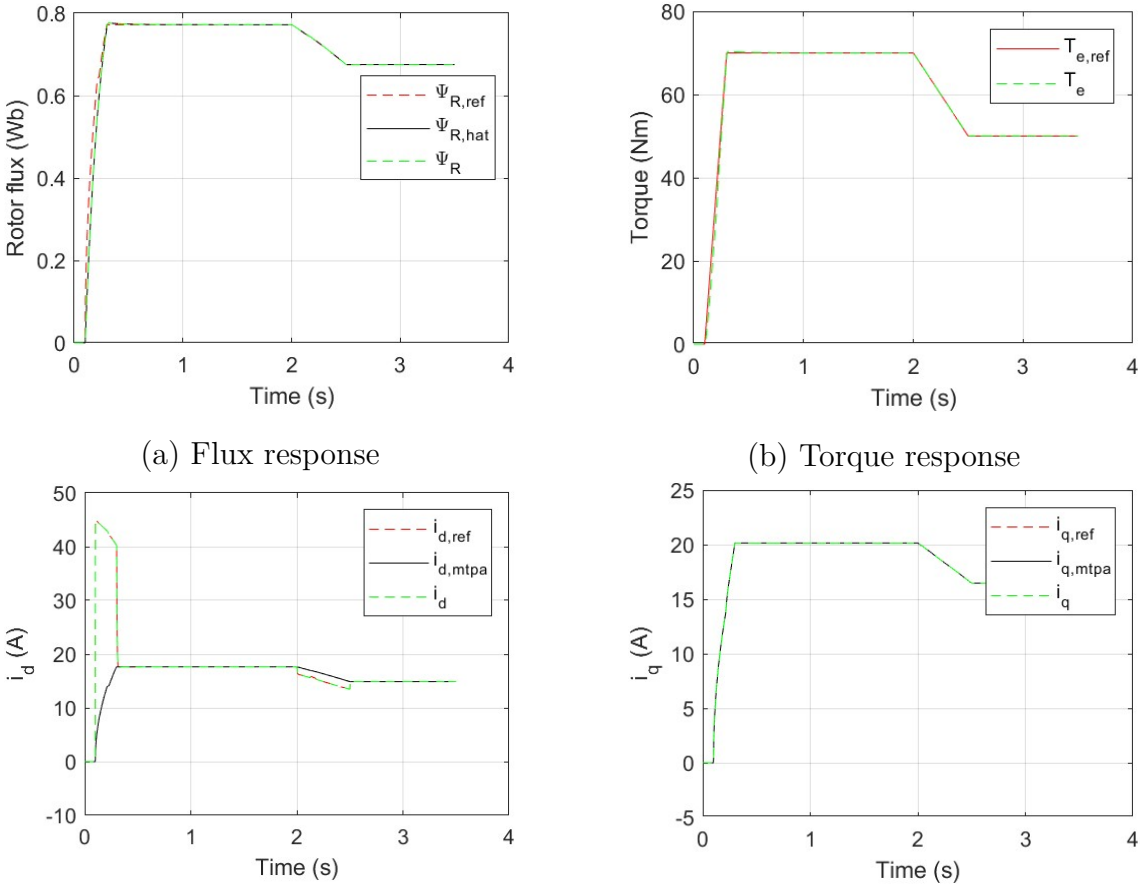

(a) Flux response

(b) Torque response

(c) i_{sd} response

(d) i_{sq} response

Figure 5.4: Machine and current response to a downtrend for Strategy 1

Table 5.4: Results data for torque request decrease of 20 Nm for Strategy 1

Torque request decrease from 70 Nm to 50 Nm	**Strategy - 1**			
	Energy losses (kJ)	**Stator Power (kW)**	**Shaft Power (kW)**	**Power Losses (%)**
	0.770	**2.82**	**2.61**	**7.44**

Upon simulating for Strategy 2 shown in Figure 5.5, it is observed that the torque request is met perfectly for the large ramp as well as the small ramp observed in Figure 5.5 (b), while the flux response lags initially for the large torque ramp due to being limited by the current magnitude available in this strategy. However the flux response is perfect for the small ramp due the availability of more current magnitude for the decrease in torque request as shown in Figure 5.5 (a). The results for the energy losses, stator power, shaft power and power losses for Strategy 2 for torque request decrease of 20 Nm are shown in Table 5.5. The stator and shaft powers are given after the torque request decrease, for the final value in Figure 5.5. The energy loss is the power losses, stator power subtracted with shaft power, integrated from 0s to 3.5s.

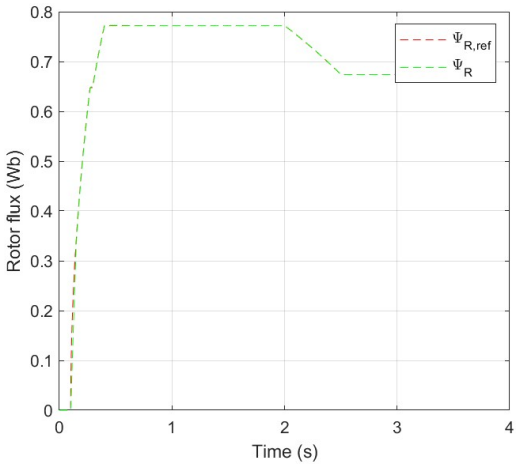

(a) Flux response

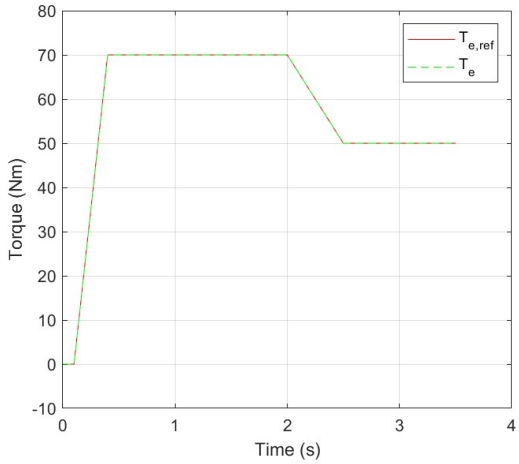

(b) Torque response

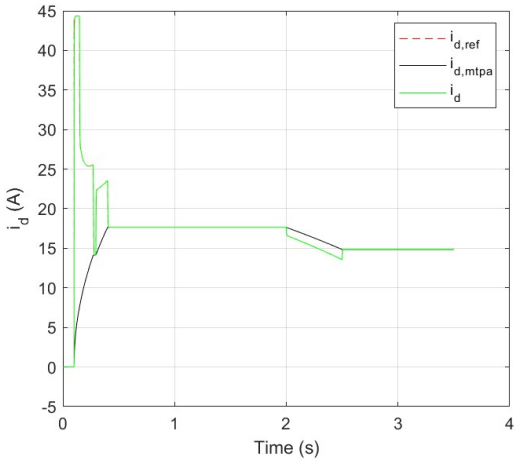

(c) i_{sd} response

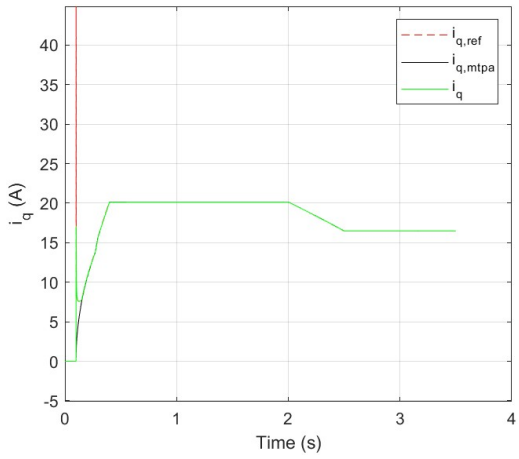

(d) i_{sq} response

Figure 5.5: Machine and current response to a downtrend for Strategy 2

Table 5.5: Results data for torque request decrease of 20 Nm for Strategy 2

Torque request decrease from 70 Nm to 50 Nm	**Strategy - 2**			
	Energy losses (kJ)	**Stator Power (kW)**	**Shaft Power (kW)**	**Power Losses (%)**
	0.770	**2.82**	**2.61**	**7.44**

Strategy 3 for this test case yields similar results to that of Strategy 3 for a torque request increase above the steady state operating point, explained earlier in Section 5.1. The plots for Strategy 3 for the case of torque request decrease of 20 Nm below the steady state operating point are shown in Figure 5.6. The reason for the spike in i_{sd} at 0.1s in Figure 5.6(c) remains the same as the reason for the spike in i_{sd} at 0.1s in Figure 5.3(c). The results for the energy losses, stator power, shaft power and power losses for Strategy 3 for torque request decrease of 20 Nm are shown in Table 5.6. The stator and shaft powers are given after the torque request decrease,

for the final value in Figure 5.6. The energy loss is the power losses, stator power subtracted with shaft power, integrated from 0s to 3.5s.

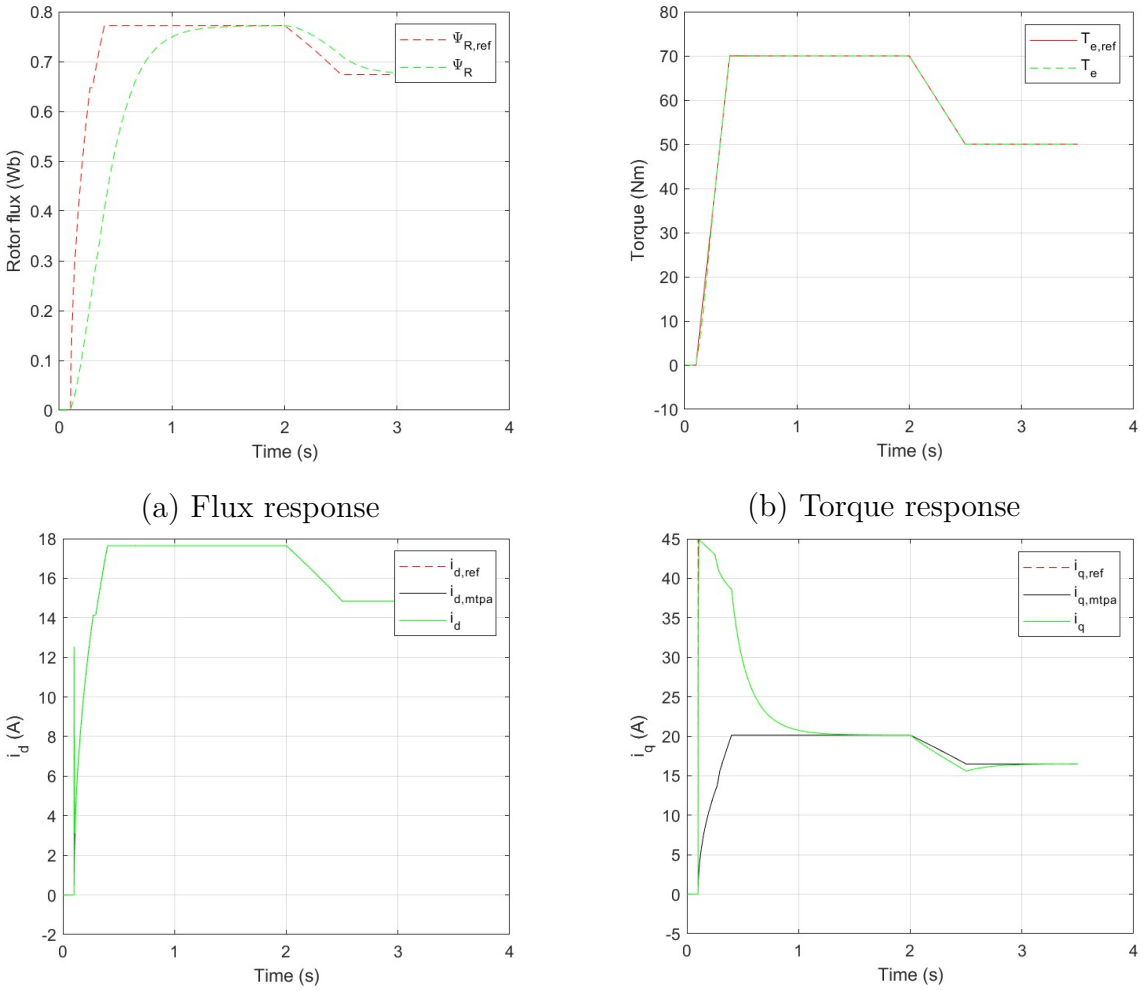

(a) Flux response

(b) Torque response

(c) i_{sd} response

(d) i_{sq} response

Figure 5.6: Machine and current response to a downtrend for Strategy 3

Table 5.6: Results data for torque request decrease of 20 Nm for Strategy 3

Torque request decrease from 70 Nm to 50 Nm	**Strategy - 3**			
	Energy losses (kJ)	**Stator Power (kW)**	**Shaft Power (kW)**	**Power Losses (%)**
	0.919	**2.82**	**2.61**	**7.44**

Upon simulating for Strategies 1, 2 and 3, it is observed that the flux controller is capable of meeting the small torque ramp requests from a steady state operating point with any of the strategies but there is a difference between the three strategies when it comes to meeting the large torque ramp request. Between Strategies 1 & 2 the large torque request ramp is met perfectly in the second strategy as we are able

to boost both currents i_{sd} and i_{sq} as opposed to boosting only i_{sd} in Strategy 1.

From the point of Joule losses it can be said that the strategies in which the currents deviate away from the MTPA trajectory for a longer duration and utilise the maximum current magnitude for a longer time will lead to more energy consumption and therefore higher Joule losses. Hence in this test case, both Strategies 1 & 2 would be ideal for a small torque request increase above a steady state operating point, as both the strategies have the same energy consumption's and power losses as shown in Tables 5.1, 5.2, and 5.3.

For the case of a small torque request decrease below the steady state operating point, both Strategies 1 & 2 are ideal as well since they have the same energy consumption and power losses leading to the least amount of Joule losses as shown by data in Tables 5.4, 5.5, and 5.6.

The general behaviour of Strategy 3 strategy is that i_{sq} must deviate away from its MTPA trajectory for a very long duration while i_{sd} follows its MTPA trajectory, thereby utilizing the maximum current magnitude available leading to an increased energy consumption and thereby contributing to higher Joule losses compared to the other 2 strategies. The higher Joule losses can be seen for the tests of the small torque increase and decrease of 20 Nm by comparing the energy loss values in Tables 5.1, 5.2, 5.3, 5.4, 5.5 and 5.6 where the energy loss for Strategy 3 is 15 % to 19 % higher for these tests. Hence this strategy is discarded for further test cases.

5.2 Field Weakening

In this test case, the machine is operating constantly at 1200 RPM, which is above the knee-point in Figure 3.3. The machine is subjected to a torque profile $T_{e,ref}$ as shown in Figure 5.7 (b) where the flux response is managed by a flux controller, and the torque response follows the $i_{sq,MTPA}$ trajectory. Initially, during the torque ramp-up, i_{sd} increases rapidly as seen in Figure 5.7 (c), which helps the machine adjust its magnetic flux quicker than if it were following the $i_{sd,MTPA}$ trajectory. This quick change in flux contributes to the rise in back-emf. In (2.10), it is observed that the rise in i_{sd} alongside the corresponding increase in flux as noticed in Figure 5.7 (a), results in a large value of u_{sq} which comes from the cross-coupling term $\omega_1 L_\sigma i_{sd}$ and the back-emf term $\omega_r \psi_R$ becoming larger, eventually leading to the voltage hitting its limit and causing a loss of control, which results in an undesirable torque response. This can be noticed in figure around 0.36s into the simulation, there is a sharp variation in the T_e trajectory. This variation is linked to a sudden drop in i_{sq}, as shown in Figure 5.7 (d), which is caused by that the voltage limit is reached and the controllability of the currents are lost. This behaviour can be better understood by examining the voltage behaviour in Figure 5.8 at the 0.36s mark, where the voltage magnitude is limited to the converter's maximum voltage of 250V.

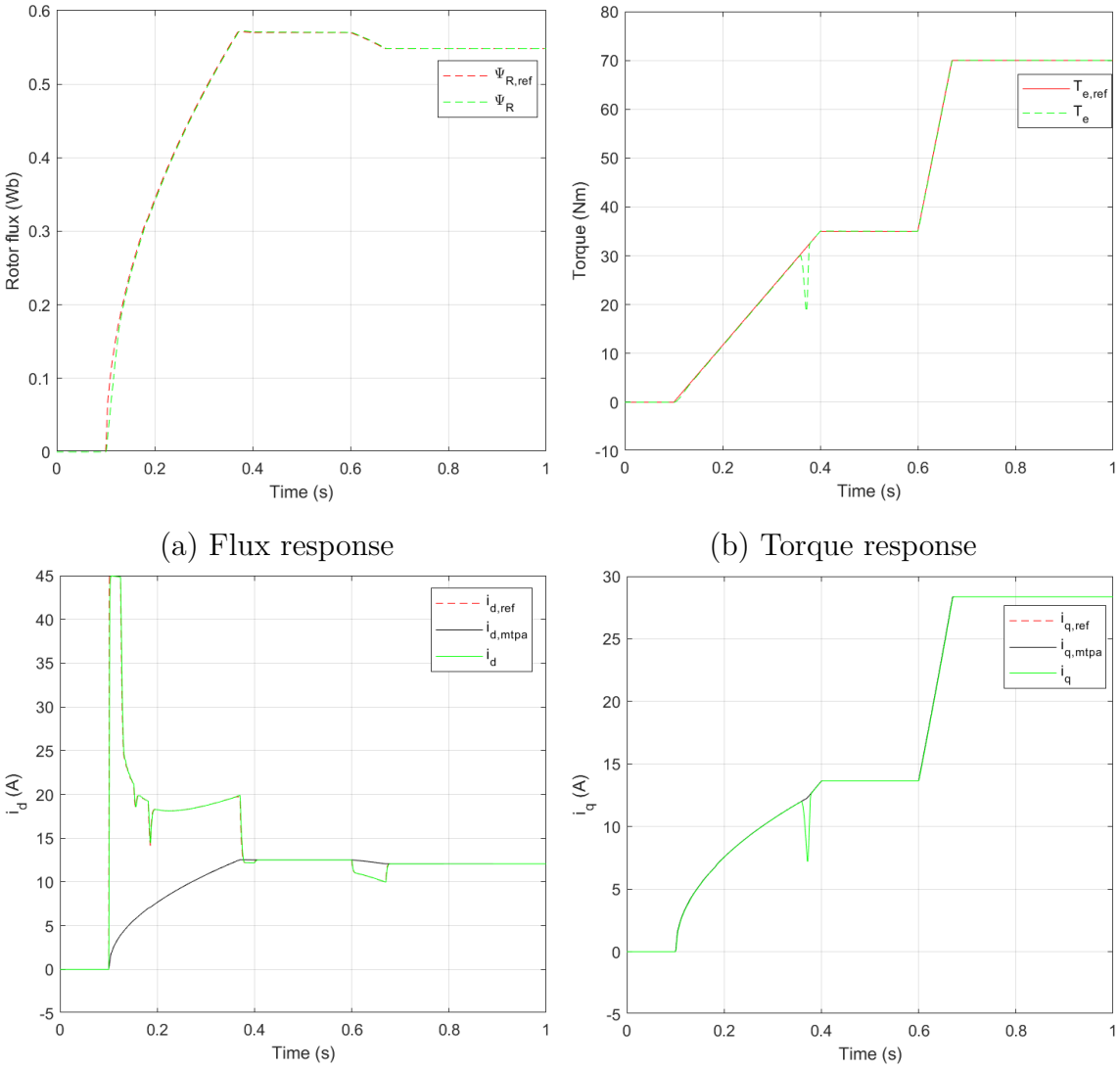

(a) Flux response

(b) Torque response

(c) i_{sd} response

(d) i_{sq} response

Figure 5.7: Machine and current response in the Field Weakening region using Strategy 1

This explains why the sharp decrease in i_{sq} is observed, highlighting a limitation of using Strategy 1 at high machine speeds. One approach to overcome this limitation is to implement a Field Weakening controller that intentionally limits the stator current component responsible for generating magnetic flux (i_{sd}). By reducing i_{sd}, the controller lowers the back-emf, which in turn reduces the stator voltage, ensuring it stays slightly below the converter's maximum limit. This buffer is essential for maintaining control and stability as it prevents the voltage from reaching a level where the control system could lose its ability to regulate the machine effectively.

The Field Weakening controller is designed with a field weakening voltage limit ($V_{s,fw}$) that is intentionally set lower than the converter's maximum voltage limit ($V_{s,max}$). Its primary objective is to adjust the machines flux level based on speed,

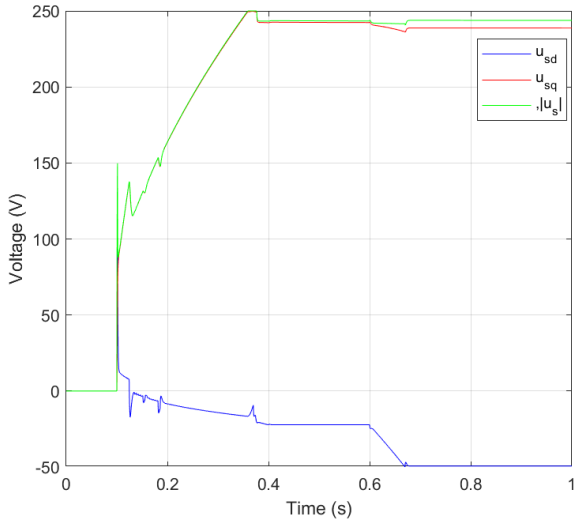

Figure 5.8: Voltage response in the Field Weakening region using Strategy 1

ensuring that it remains within a range suitable for this lower field weakening voltage limit. The difference between $V_{s,max}$ and $V_{s,fw}$ creates a buffer which is crucial for the controllability of the currents.

In a cascaded control system, the Field Weakening controller algorithm reads the reference dq voltage magnitude from the current controller and compares it to a predefined $V_{s,fw}$ [14]. Based on the remaining voltage margin within this buffer, the controller calculates and outputs a new flux reference $\psi_{R,ref}$ that can be maintained within the field weakening voltage limit. Using this approach, it is seen from Figure 5.9 (d) that the deviation of i_{sq} which was earlier noticed in Figure 5.7 (d) is eliminated. In this case, the $V_{s,max}$ is 250V while the $V_{s,fw}$ is set slightly lower at 235V, creating a 15V controllability buffer.

As seen in Figure 5.10, once the machine enters field weakening region, which occurs after 0.4s of simulation time, the Field Weakening controller actively adjusts $\psi_{R,ref}$ to prevent the stator voltage from exceeding $V_{s,fw}$. This is achieved by lowering the flux in the machine below the reference value, as can be seen in Figure 5.9 (a). When comparing the flux responses in Figure 5.7 (a) and 5.9 (a), it is evident that the flux decrease in the latter is much quicker between 0.4s and 0.8s, indicating a faster reduction in the back-emf term. This helps keep the stator voltage within $V_{s,fw}$. However, the rapid decrease in ψ_R leads to a corresponding loss of torque as seen from Figure 5.9 (b). To compensate for this loss in torque, Startegy 2 can be used along with the Field Weakening controller. The energy and power loss data for Strategy 1 using Field Weakening controller is presented in Table 5.7. The stator and shaft powers are given for the final value in Figure 5.9. The energy loss is the power losses, stator power subtracted with shaft power, integrated from 0s to 1s.

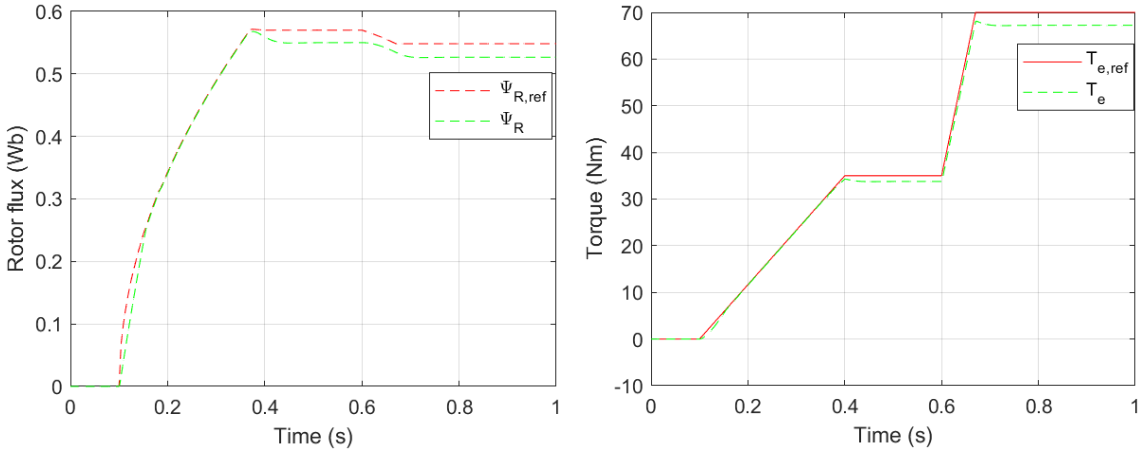

(a) Flux response

(b) Torque response

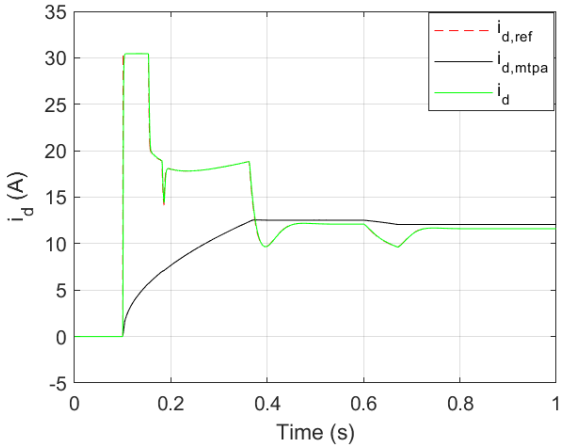

(c) i_{sd} response

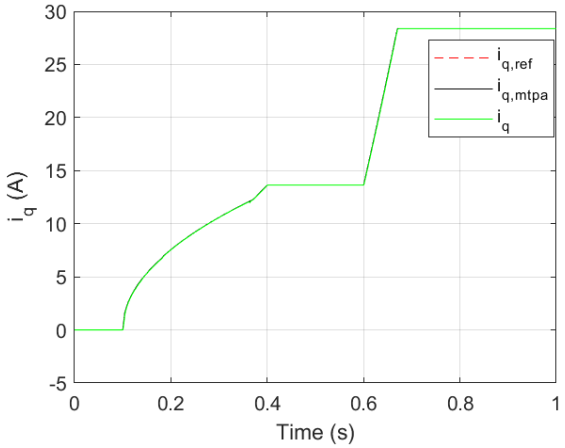

(d) i_{sq} response

Figure 5.9: Machine and current response with field weakening controller using Strategy 1

Table 5.7: Energy and Power loss data for Field Weakening controller using Strategy 1

Field Weakening controller	Strategy - 1			
	Energy losses (kJ)	Stator Power (kW)	Shaft Power (kW)	Power Losses (%)
	0.195 kJ	8.91	8.45	5.16

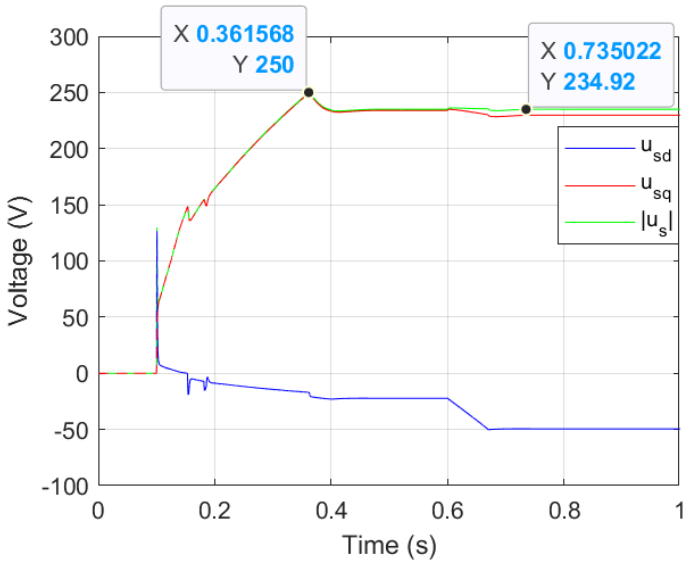

Figure 5.10: Voltage response with field weakening controller using Strategy 1

It can be seen in Figure 5.11 that using Strategy 2 together with the Field Weakening controller results in a more accurate torque response compared to that of Strategy 1. In the field weakening region, which occurs after 0.4s of the simulation time, i_{sq} is boosted whenever ψ_R is below its reference value. However, this means a higher utilisation of current and the deviation from the MTPA trajetory contribute to higher Joule losses, as seen in Table 5.8. In the table , the energy and power loss data for Strategy 2 using Field Weakening controller is shown. The stator and shaft powers are given for the final value in Figure 5.11. The energy loss is the power losses, stator power subtracted with shaft power, integrated from 0s to 1s.

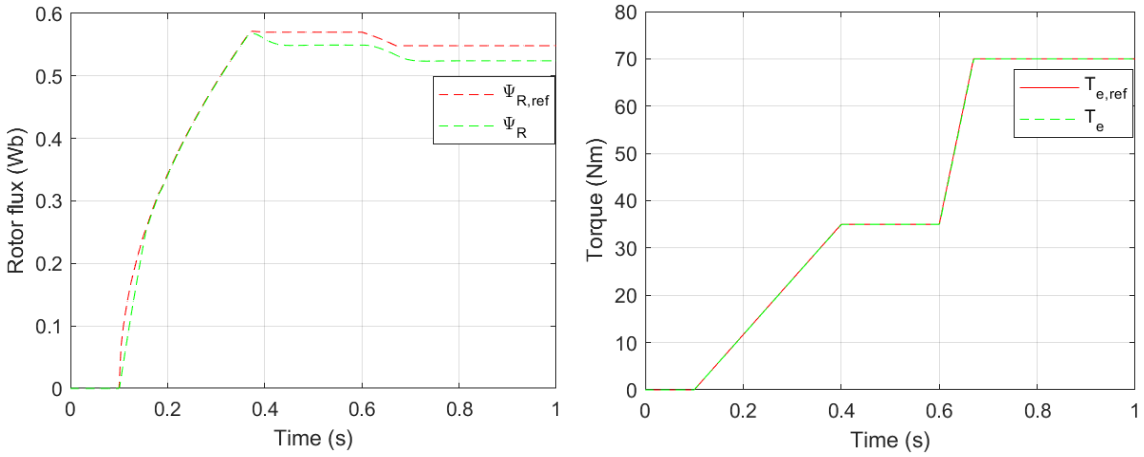

(a) Flux response

(b) Torque response

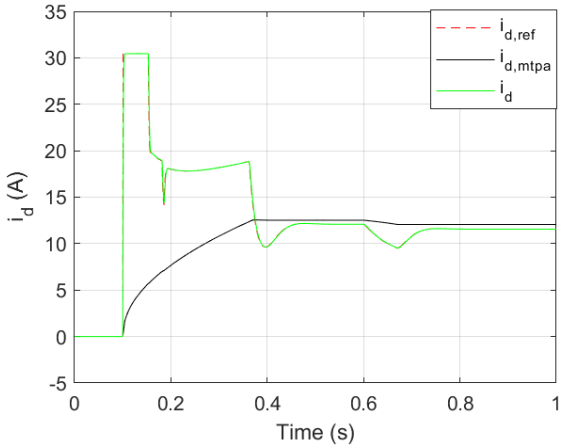

(c) i_{sd} response

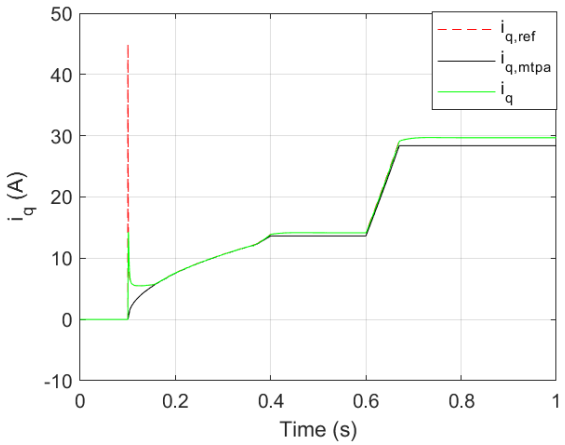

(d) i_{sq} response

Figure 5.11: Machine and current response with field weakening controller using Strategy 2

Table 5.8: Energy and Power loss data for Field Weakening controller using Strategy 2

Field Weakening controller	Strategy - 2			
	Energy losses (kJ)	Stator Power (kW)	Shaft Power (kW)	Power Losses (%)
	0.206 kJ	9.3	8.79	5.48

To analyse the machine's response during a downtrend in the field weakening region, the torque is stepped down from 70 Nm to 5 Nm, as shown in Figure 5.12 (b). This sudden decrease in torque requires a rapid reduction in flux. However, after the torque request has started to drop, it can be observed from Figure 5.12 (a), the rotor flux ψ_R remains higher than its reference $\psi_{R,ref}$ after 1s of simulation, indicating that the flux reduction is slower than expected.

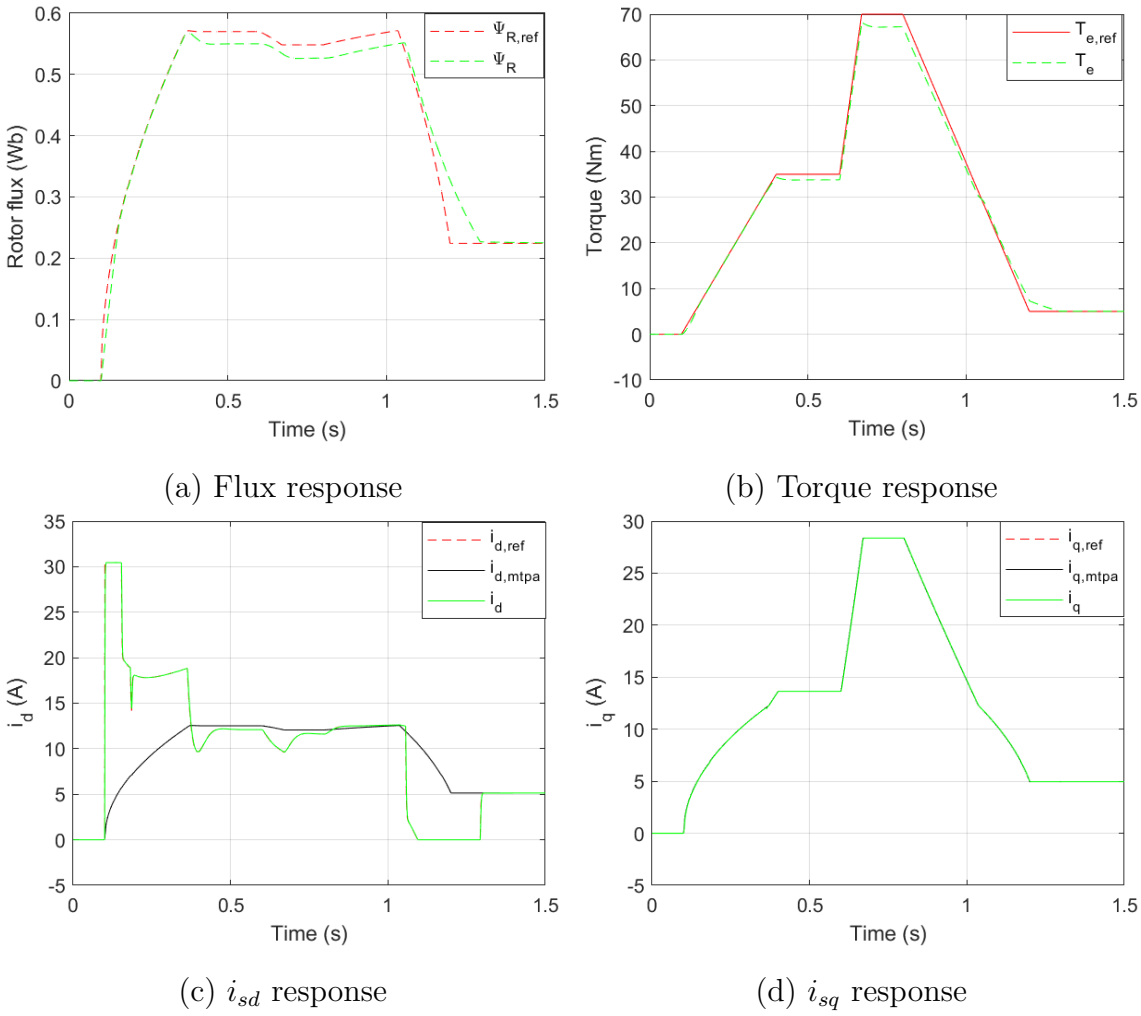

(a) Flux response

(b) Torque response

(c) i_{sd} response

(d) i_{sq} response

Figure 5.12: Machine and current response with field weakening controller to negative torque slope using Strategy 1

Table 5.9: Energy and Power loss data with field weakening controller using Strategy 1

Negative torque slope	Strategy - 1			
	Energy losses (kJ)	Stator Power (kW)	Shaft Power (kW)	Power Losses (%)
	0.189 kJ	0.651	0.63	3.22

This slow response can be attributed to the minimum limit set for i_{sd} in the flux controller, which is configured to 0A for this test case. This limit is reached when the flux in the machine has to be reduced quickly as seen in Figure 5.12 (c). However, a slow decay of flux is undesirable because the back-emf generated by the machine remains higher for a longer period, even when the torque demand is low, as observed between 1s and 1.5s in Figure 5.12 (a). The energy and power loss data for this test case using Strategy 1 is presented in Table 5.9. The stator and shaft powers are given for the final value in Figure 5.12. The energy loss is the power losses, stator

power subtracted with shaft power, integrated from 0s to 1.5s.

When Strategy 2 is used for same test case, the torque response is observed to be more accurate from Figure 5.13 (b). This is because i_{sq} is being controlled in a way that it compensates for a lower or higher i_{sd} to produce torque. However, this also means i_{sq} will have more deviations away from its MTPA trajectory, contributing to Joule losses. The energy and power loss data using Strategy 2 is presented in Table 5.10. The stator and shaft powers are given for the final value in Figure 5.13. The energy loss is the power losses, stator power subtracted with shaft power, integrated from 0s to 1.5s.

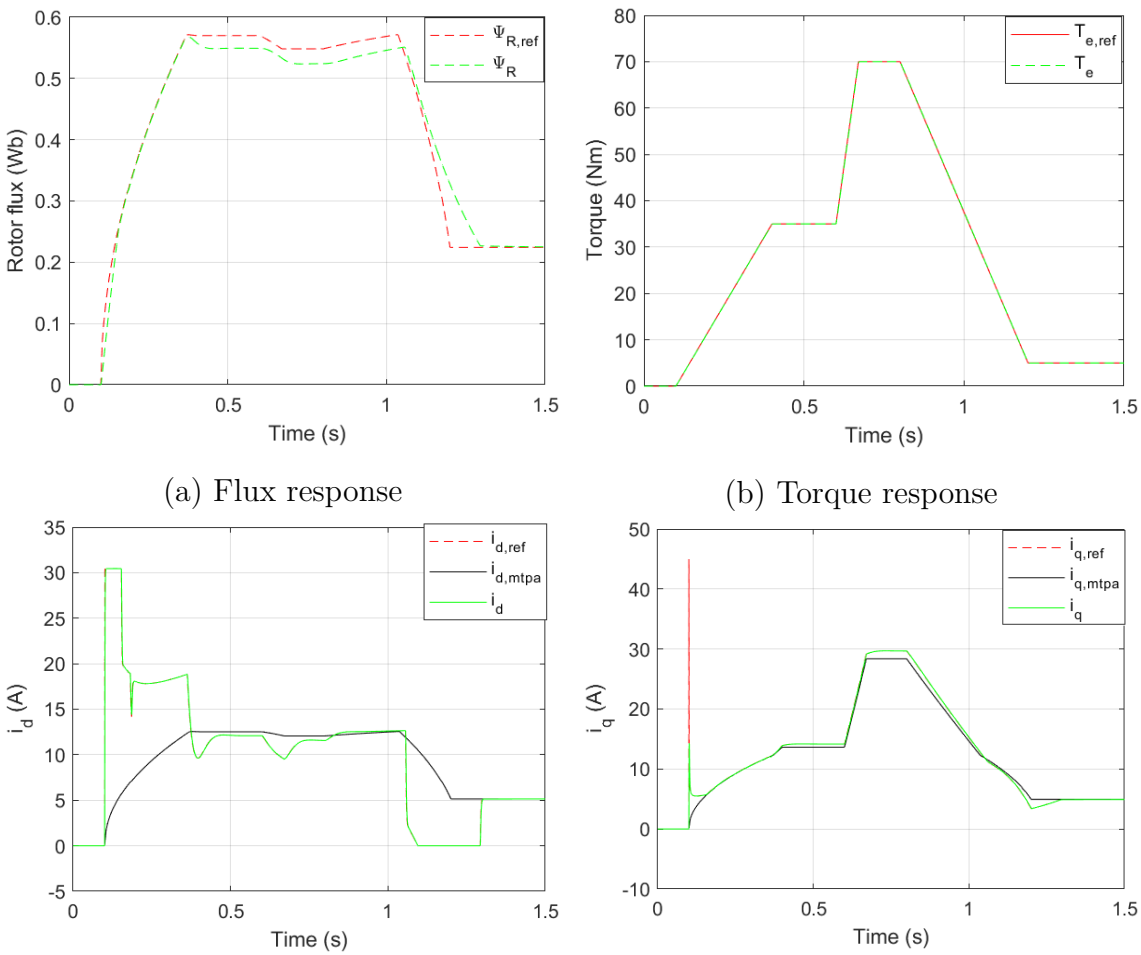

(a) Flux response

(b) Torque response

(c) i_{sd} response

(d) i_{sq} response

Figure 5.13: Machine and current response with field weakening controller to negative torque slope using Strategy 2

Table 5.10: Energy and Power loss data for field weakening controller using Strategy 2

Negative torque slope	**Strategy - 2**			
	Energy losses (kJ)	**Stator Power (kW)**	**Shaft Power (kW)**	**Power Losses (%)**
	0.197 kJ	**0.648**	**0.628**	**3.18**

Upon comparing Tables 5.9 and 5.10, it can be observed that using Strategy 2 results in higher energy losses due to the fact that both currents deviate from their MTPA trajectories. However, the torque response is more accurate with Strategy 2. The power losses in Strategy 2 are slightly lower than Strategy 1 because of the deviations of i_{sq} below its MTPA trajectory, which is noticeable in Figure 5.13 (d) after 1s of the simulation time.

5.3 Tracing the Torque-Speed curve boundary

To conclude the study, a hard acceleration scenario from standstill to the maximum machine speed is simulated. In a real-world context, this could represent accelerating from standstill to the vehicle's top speed on a highway. This scenario is set to occur in 8s as illustrated in Figure 5.14 where the machine speed increases from 0 to maximum speed in 8s. The torque is ramped up from 0 Nm to maximum in 0.5s and is then maintained at the maximum torque available at the current speed of the machine. The torque request follows Figure 3.3, as can be seen in Figure 5.15 (b).

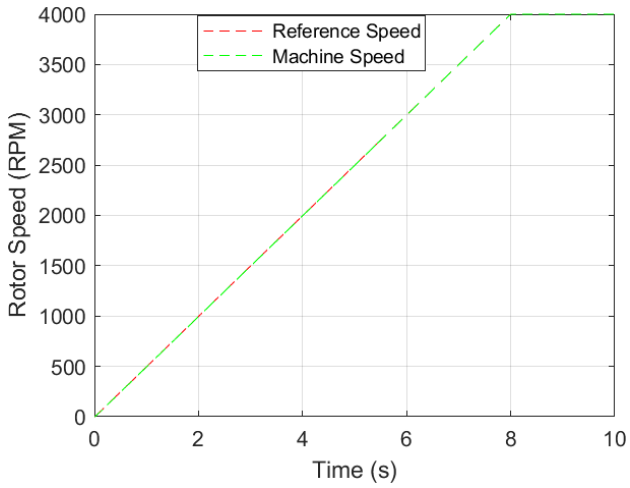

Figure 5.14: Plot showing the acceleration

When this scenario is simulated with a Field Weakening controller using Strategy 1, the torque response shows a slight lag compared to its reference between 2.5s and 6s, as illustrated in Figure 5.15. This lag in torque response occurs during this time because, the machine has entered its field weakening region and operates at a lower flux level. The Field Weakening controller is actively adjusting the flux reference in the machine based on its operating speed and the available voltage ($V_{s,fw}$) for controlling the currents. During this period, i_{sq} follows its MTPA trajectory, hence the torque output is lagging because the rotor flux ψ_R, which is adjusted by the field weakening controller is lower than its reference $\psi_{R,ref}$. This reduced flux directly diminishes the torque output. The data related to energy and power losses for the highway acceleration test case using Strategy 1 is presented in Table 5.11. The stator and shaft powers are given for the final value in Figure 5.15. The energy loss is the power losses, stator power subtracted with shaft power, integrated from 0s to 10s.

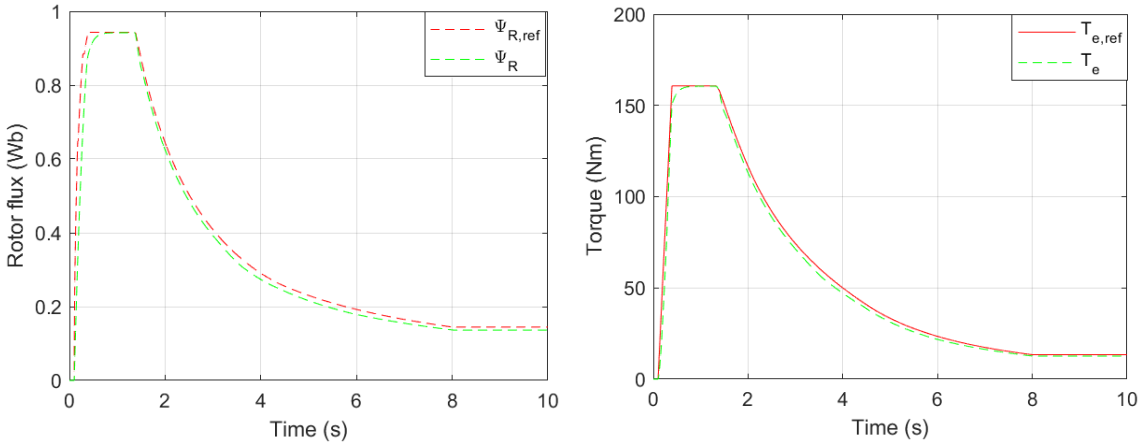

(a) Flux response

(b) Torque response

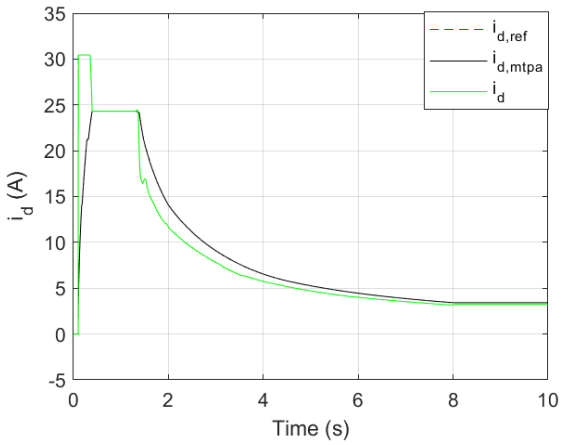

(c) i_{sd} response

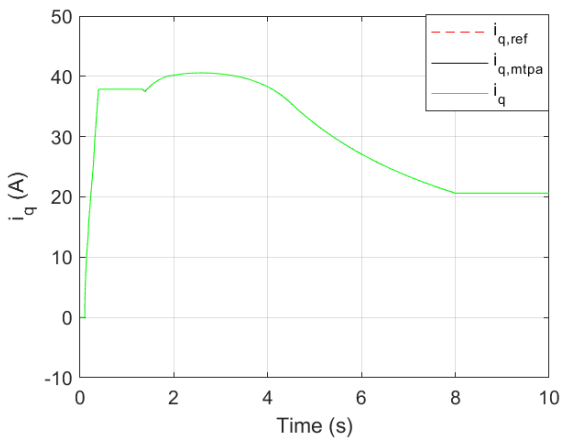

(d) i_{sq} response

Figure 5.15: Machine response to highway acceleration from standstill using Strategy 1

Table 5.11: Energy and Power loss data for highway acceleration test using Strategy 1

Highway acceleration	Strategy - 1			
	Energy losses (kJ)	Stator Power (kW)	Shaft Power (kW)	Power Losses (%)
	3.84 kJ	5.53	5.3	4.16

Using Strategy 2 for the same test case, the torque response is more accurate compared to Strategy 1, as seen in Figure 5.16 (b). During the 2.5s to 6s simulation window, Figure 5.16 (a) indicates that the field weakening is higher with Strategy 2 than with Strategy 1. This increased field weakening is directly related to the boosting of i_{sq} above its MTPA value during this period, which demands a higher voltage for control. To accommodate this requirement, the field weakening controller further reduces the flux to minimize the voltage drop caused by back-emf and ensuring the stator voltage magnitude does not exceed $V_{s,fw}$, thereby maintaining effective

control over the currents during this time. The data related to energy and power losses for the highway acceleration test case using Strategy 2 is presented in Table 5.12. The stator and shaft powers are given for the final value in Figure 5.16. The energy loss is the power losses, stator power subtracted with shaft power, integrated from 0s to 10s.

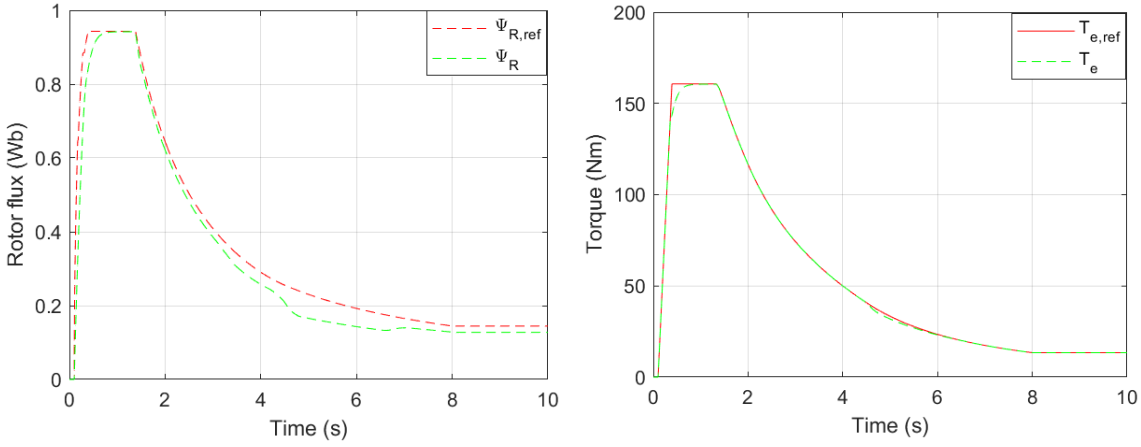

(a) Flux response

(b) Torque response

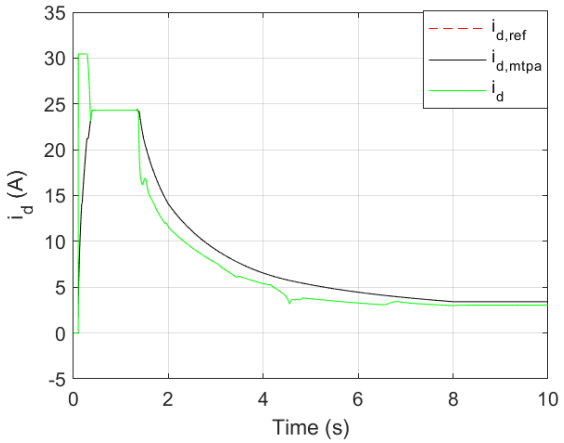

(c) i_{sd} response

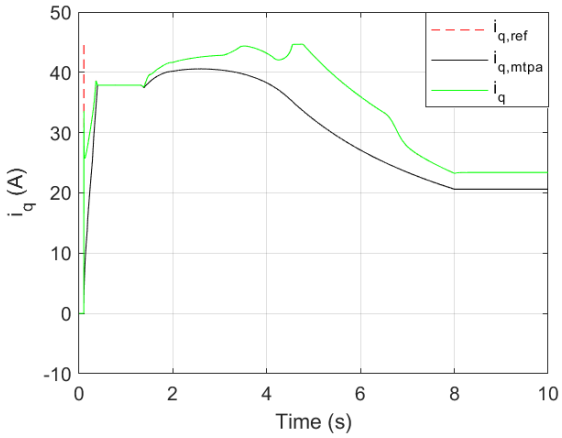

(d) i_{sq} response

Figure 5.16: Machine response to highway acceleration from standstill using Strategy 2

Table 5.12: Energy and Power loss data for highway acceleration test using Strategy 2

Highway acceleration	**Strategy - 2**			
	Energy losses (kJ)	**Stator Power (kW)**	**Shaft Power (kW)**	**Power Losses (%)**
	4.79 kJ	**5.91**	**5.62**	**4.90**

6
Conclusions and future work

In this chapter, the findings from experimentation of the proposed control strategies are summarised and it conveys the benefits and drawbacks of each of them. It includes the section of future work where points related to widening the study are discussed. Within this chapter, general term losses is used to represent both copper and iron losses in the machine.

6.1 Conclusions

Operating at MTPA points is effective for minimizing Joule losses and reducing overall energy consumption as the currents are optimized for maximum efficiency. However, the transient response is slower because MTPA operation does not use the rated current magnitude but a trajectory that is optimised to reduce Joule losses, leading to a slower dynamic response. This slower response, as discussed in Subsection 4.1.2 is particularly undesirable in automotive drive system applications where a fast and dynamic response is essential. Therefore, while MTPA is beneficial for efficiency, it may not fully meet the demands of a high performance automotive drive systems, where a balance between efficiency and responsiveness is necessary.

Using Strategy 1 in the constant torque region reveals that the torque response initially lags behind its reference when starting from standstill during high acceleration scenarios, such as a steep torque ramp. This lag occurs because the machine is demagnetized at standstill and requires time for the flux to build up. However, for small variations in torque ramps from a steady-state operating point, the torque response accurately tracks its reference with this strategy. When combining this strategy with a Field Weakening controller, a lagging torque response is observed during field weakening. This lag is due to the machine operating at a lower flux level lower than its reference, causing the torque to drop.

Using Strategy 2 in the constant torque region effectively overcomes the limitations encountered with Strategy 1. Although there is a slight initial lag in flux buildup compared to its reference, the increase in i_{sq} above its MTPA trajectory compensates for the resulting torque drop, ensuring a more responsive performance. This strategy also proves effective for small variations in torque ramps from a steady-state operating point. When applied with a Field Weakening controller, Strategy 2 successfully mitigates the drop in torque during field weakening. However, this improvement comes at the cost of higher energy losses, as the strategy prioritizes

responsiveness over efficiency.

Using Strategy 3 reveals that while the flux response significantly lags behind its reference, the torque response remains quick. This response is achieved by increasing i_{sq} above its MTPA value during most of the transient period. For small variations in torque ramps from a steady-state operating point, this strategy delivers accurate torque control. However, this approach results in the highest energy losses across various operating points. This is because both i_{sd} and i_{sq} are increased above their MTPA trajectory during transients and continuing until a steady-state is reached. Due to its inefficiency characterized by these elevated energy losses, Strategy 3 is not considered in the discussions.

The analysis of energy and power losses across the three strategies reveals that Strategies 1 and 2 exhibit similar energy and power losses. However, Strategy 3 incurs significantly higher energy losses to produce the same shaft power as Strategies 1 and 2, making it the least preferred option.

The choice between Strategy 1 and Strategy 2 depends on the desired performance requirement. If precise torque control is required for both high and small accelerations, Strategy 2 is the better choice due to its ability to maintain accurate torque response under varying conditions. Conversely, if high acceleration is not a primary concern but maintaining a perfect response to small accelerations is important, then Strategy 1 is more suitable.

6.2 Future Work

Some of the aspects that can be included into the future work are

- To study the transient behavior in more detail, it would be beneficial to consider the mechanical dynamics of the machine by incorporating advanced inertia models. This approach enables the study of the impact of speed oscillations on machine control.

- Introducing parameter estimation error can be helpful to study the sensitivity of each strategy in more detail.

- Adding a Finite Element Analysis dimension widens the scope and reveals the contribution and exact nature of losses occurring with different strategies.

- Finally, to test the robustness and accuracy of the machine model and control strategies, simulated data can be compared with test data obtained from physical tests on a test rig. This comparison will help validate the model and improve its reliability.

Bibliography

[1] B. Amin, “Induction Motors in Transient Regimes”, in Oscillatory Stability of Converter-Dominated Power Systems, Oscillatory Stability of Converter-Dominated Power Systems, 2001, pp. 95–108. doi: 10.1007/978-3-662-04373-85.

[2] J. A. Santiseban and R. M. Stephan, “Vector control methods for induction machines: an overview”, IEEE Transactions on Education, vol. 44, no. 2, pp. 170–175, 2001, doi: 10.1109/13.925828.

[3] S. Bozhko, S. Dymko, S. Kovbasaand S. M. Peresada, “Maximum Torque-per-Amp Control for Traction IM Drives: Theory and Experimental Results”, IEEE Transactions on Industry Applications, vol. 53, no. 1, pp. 181–193, 2017, doi: 10.1109/tia.2016.2608789.

[4] C. Attaianese, M. Di Monaco, I. Spinaand G. Tomasso, “A Variational Approach to MTPA Control of Induction Motor for EVs Range Optimization”, IEEE Transactions on Vehicular Technology, vol. 69, no. 7, pp. 7014–7025, 2020, doi: 10.1109/tvt.2020.2983908.

[5] G. R. Slemon, “Modelling of induction machines for electric drives”, IEEE Transactions on Industry Applications, vol. 25, no. 6, pp. 1126–1131, 1989, doi: 10.1109/28.44251.

[6] Abdul, Ali & Altahir, Ali. (2020). "Park and Clark Transformations Park and Clark Transformations: A Short Review." doi: 10.13140/RG.2.2.20287.46241.

[7] Parton, J. E., "A general theory of phase transformation," Proc.I.E.E., Vol. 99, Part IV, 1952, pp. 12-23.

[8] M. Hrkel, J. Vittekand Z. Biel, “Maximum torque per ampere control strategy of induction motor with iron losses”, 2012. doi: 10.1109/elektro.2012.6225635.

[9] Z. Peng, “Analysis and Implementation of Constrained MTPA Criterion for Induction Machine Drives”, IEEE Access, vol. 8, pp. 176445–176453, 2020, doi: 10.1109/access.2020.3024195.

[10] The MathWorks, Inc. “Optimization Toolbox Documentation” mathworks.com. Accessed: June 06, 2024. [Online]. Available:

https://se.mathworks.com/help/optim/ug/fmincon.html

[11] The MathWorks, Inc. "Optimization Toolbox Documentation" mathworks.com. Accessed: June 06, 2024. [Online]. Available: https://se.mathworks.com/help/optim/ug/fsolve.html

[12] A. A. H. Khamis, A. M. A. Abbasand M. A. M. Algoul, "Comparative Study Between a Novel Direct Torque Control and Indirect Field Oriented Control of Three-Phase Induction Motors", 2022. doi: 10.1109/mi-sta54861.2022.9837649.

[13] Harnefors, Lennart, Control of variable-speed drives, Applied Signal Processing and Control, Department of Electronics, Mälardalen University, Västerås, 2002

[14] G. Gallegos-Lopez, F. S. Gunawanand J. E. Walters, "Current Control of Induction Machines in the Field-Weakened Region", 2006. doi: 10.1109/ias.2006.256491.